DEVELOPMENT OF AUTOMATED METHOD OF OPTIMIZING STRENGTH OF SIGNAL RECEIVED BY LASER INTERFEROMETER

A Thesis
Presented to
The Academic Faculty

by

Tyler W. Randolph

In Partial Fulfillment
of the Requirements for the Degree
Master of Science in the
School of Mechanical Engineering

Georgia Institute of Technology
August 2009

DEVELOPMENT OF AUTOMATED METHOD OF OPTIMIZING STRENGTH OF SIGNAL RECEIVED BY LASER INTERFEROMETER

Approved by:

Dr. I. Charles Ume , Advisor
School of Mechanical Engineering
Georgia Institute of Technology

Dr. Nader Sadegh
School of Mechanical Engineering
Georgia Institute of Technology

Dr. J. Rhett Mayor
School of Mechanical Engineering
Georgia Institute of Technology

Date Approved: June 8, 2009

ACKNOWLEDGMENTS

There are many people who laid the foundation for the work in this thesis. Most of all, the former and current students who have worked in the Laser Ultrasonic Research Lab at Georgia Institute of Technology have turned an idea into a working inspection system.

My advisor, Dr. I. Charles Ume, gave me the opportunity and the liberty to learn and explore my own research goals while supporting and advising me. For his insights, professionalism, and encouragement, I am very grateful.

Special thanks are due to the Department of Mechanical Engineering for the use of the resources of the machine shop and electronic laboratory, which assisted in the development of the mechanical and electrical hardware.

This work was supported under a National Science Foundation grant. Any opinions, findings, or conclusions are that of the author, and not necessarily that of the National Science Foundation.

I would like to especially thank my mother and father, without whose guidance and support I would not be here.

TABLE OF CONTENTS

LIST OF FIGURES

SUMMARY

The long-term goal of this research is to assist in the development of a fast, accurate, and low-cost nondestructive inspection prototype for solder joints in integrated circuits (IC). The goal of the work described in this thesis is to develop a fully automated system to maintain the signal strength of the vibrometer that would reduce the testing time while maintaining or improving the quality of the defect detection results. The ability to perform the inspections in an automated manner is very important in order to demonstrate the ability of the defect detection system to be used for online inspection without the need of an operator. The system was able to find the maximum signal strength (at a single point on the surface of a flip chip) nearly five times faster than Polytec's commercial system with a search time of approximately 2.1 sec. When integrated into the nondestructive inspection prototype, the system described in this work was found to approximately reduce the data acquisition time per test location by four times, with a minimum data acquisition time of 8.5 sec and an average time of 15.4 sec, while maintaining the same level of quality of results obtained by a skilled operator when manually maintaining the signal strength of the vibrometer.

Hardware was developed that retrofitted a vibrometer's focusing head at the end of a fiber optic cable to a motorized linear stage. This stage controlled the standoff distance between the focusing head and the IC's surface with a fixed focal length, which allowed the spot size of the laser to be adjusted while searching for a desired signal strength. Numerous tests were conducted to determine the search parameters, which led to a search time of approximately 2.1 sec. This time was found to be dependent on the surface finish of the IC being inspected. It was also found that to achieve a desired signal intensity strength, not only does the standoff height of the focusing head, which determines the laser spot size, need to be controlled, but also the exact location on which the laser is reflecting off the IC.

CHAPTER 1

INTRODUCTION

Trends in Microelectronics

The purpose of an IC package is to provide power and signal interconnects while providing protection and heat dissipation to the electronics in the IC.[1] For most mainstream applications, ICs have used lead-frame package designs like the small-outline integrated circuit (SOIC) for power and signal distribution (which was developed in the 1980s)[2] to the printed circuit board (PCB). These packages have made surface-mount devices very popular in industry; however, they have difficulty being integrated into performance applications where a high density of interconnects is needed and where size and weight are very important factors.

Several alternative packages have emerged to address these issues and limitations to the lead-frame package design. An example of these packages is the flip chip, also known as direct chip attach (DCA), which first found commercial success in IBM's mainframe computers.[2] The flip chip uses solder bumps on the bottom side of the chip to connect to the PCB. Though the use of solder bumps to connect the PCB has many advantages over lead-frame package in size and interconnect density, there are serious concerns over thermomechanical reliability and solder joint detection due to the fact that the solder joints are hidden from view. Residual stresses on the small solder bumps after the reflow process can produce significant strain on the solder joint, leading to joint cracking and delamination.[3] The use of flip chips in high performance applications where small size and low weight is critical is expected it increase significantly as more and more products are requiring these features.[4]

Some data suggests that as many as 40% of IC package defects are due to soldering problems. Because of this, it is very important to be able to monitor the solder joint quality after its assembly to the PCB.[5] The ability to detect faults in the solder joints is not only important for quality, but when these faults are detected early, corrective

action can be taken immediately, reducing costly rework, producing a higher quality product at a lower cost.

Hidden Solder Joint Inspection Techniques

With the conventional lead-frame packages, the solder connections are clearly visible, and automated optical inspection (AOI) systems can be used to detect defects. For IC chip packages like the flip chip, inspection of the solder joints is much more difficult because the connections are hidden between the chip and the substrate. More expensive inspection techniques have to be used like automated X-ray inspection (AXI) and acoustic micro imaging (AMI), for example. For AXI, the resolution that can be achieved is high, giving it the ability to detect small defects, but AXI equipment that is found in online manufacturing settings have to have a lower resolution to achieve the required short inspection times. One example of a limitation is that small solder pads cause solder joints to have a bumped appearance, very similar to a nonwetted solder ball, making it difficult to detect that kind of common defect for AXI equipment.[6] Online manufacturing AMI equipment now claims to have the same resolution as laboratory equipment without the need to fully submerge the IC in a fluid, but instead couples through a continuous stream of fluid poring on the IC.[7] This fluid still requires that the IC be cleaned and dried; therefore, it is not a fully noncontact inspection system. Another method for inspection is in-circuit testing (ICT). With this method, electrical measurements are taken on integrated test pads on the PCB to detect shorts on the solder joints. A disadvantage to this method is that it does not detect cracks that only cause intermittent failures under thermal loading. In addition to this, for applications that are space-critical, the number of test pads is limited to the available space.

Alternate Noncontact Inspection Technique

A new alternative, noncontact, nondestructive inspection technique has been developed at Georgia Institute of Technology. This technique can detect the following: missing solder bumps, nonwetted, disbonded or cracked solder joints, and misaligned or cracked packages. With this technique, a pulsed infrared laser is directed onto the surface of the IC chip package. The rapid heating and cooling of the surface by the laser

creates elastic stress waves that propagate through the chip. This broadband, laser-generated ultrasound excites the natural modes of the vibration in the chip. A laser vibrometer then measures the out-of-plane displacement of the chip's surface at several locations. Because the solder joints are acting as mechanical constraints to the vibration produced by the laser, defects in the solder joints or chip itself will alter the chip's vibrational response. Implementing several signal processing techniques, the vibrational response of the chip is compared to the vibrational response of a well-attached chip, and different types of defects can be identified[8].

This new technique has many significant advantages over existing inspection methods. With both the excitation and measurement of the chip being done by lasers, it truly is a fully noncontact method. The excitation laser power is kept low enough not to damage the surface of the chip, making it nondestructive. This new inspection technique also gives a more direct indication of solder joint integrity by inspecting the structural vibrational response of the solder joint instead of merely looking at a picture of it, like with X-ray. Current research has shown that defects can be found from only a few measurements at set locations, making this new inspection method faster than other techniques that have to image the entire chip making it very suitable to online applications.[9]

An important aspect of this new technique is the need to maintain a strong vibrometer signal intensity strength. It has been found that the signal strength, which is the measure of the amount of light coupled back into the vibrometer focusing head, is correlated to the error in the vibration waveform, resulting in the need to adjust the vibrometer at a large percentage of the measurement locations to maintain strong signal strength[10]. Current autofocusing vibrometers take a relatively long time to refocus (approximately 10 sec for the Polytec OFV-505, for example) resulting in the need for a higher speed system to maintain signal intensity strength.

Improvements Made to Original Measurement Inspection Prototype

The goal of the work described in this thesis is to develop a fully automated system to maintain the signal strength of the vibrometer that would reduce the testing time while maintaining or improving the quality of the defect detection results. To arrive

at this goal, the development of an automated system that maintains the signal intensity strength was developed. The system was able to find the maximum signal strength (at a single point on the surface of a flip chip) nearly five times faster than Polytec's commercial system with a search time of approximately 2.1 sec. When integrated into the non-destructive inspection prototype, the system described in this work was found to approximately reduce the data acquisition time per test location by four times, with a minimum data acquisition time of 8.5 sec and an average time of 15.4 sec, while maintaining the same level of quality of results obtained by a skilled operator when manually maintaining the signal strength of the vibrometer.

In the next chapter, (Chapter 2) the original inspection prototype will be described in more detail and its limitations will be addressed, showing the need for an automated system to maintain the vibrometer's signal intensity strength. Chapter 3 discusses the hardware that was developed for the system and the algorithm that was used for maintaining the signal intensity strength, along with the tests that were performed to determine the algorithm's parameters. The repeatability testing will be described and the results analyzed in Chapter 4. Chapter 5 will describe the validation testing that was conducted to show the ability for the automated system described in this work to assist in the detection of defects when integrated into the nondestructive inspection prototype. Conclusions on the advantages and limitations of the system are the subject of Chapter 6. Finally, areas of future work that would be beneficial to the system will be described in Chapter 7.

CHAPER 2

EXAMINATION OF ORIGINAL MEASUREMENT PROTOTYPE

The nondestructive inspection system that was developed at Georgia Institute of Technology is shown in Figure 2.1.

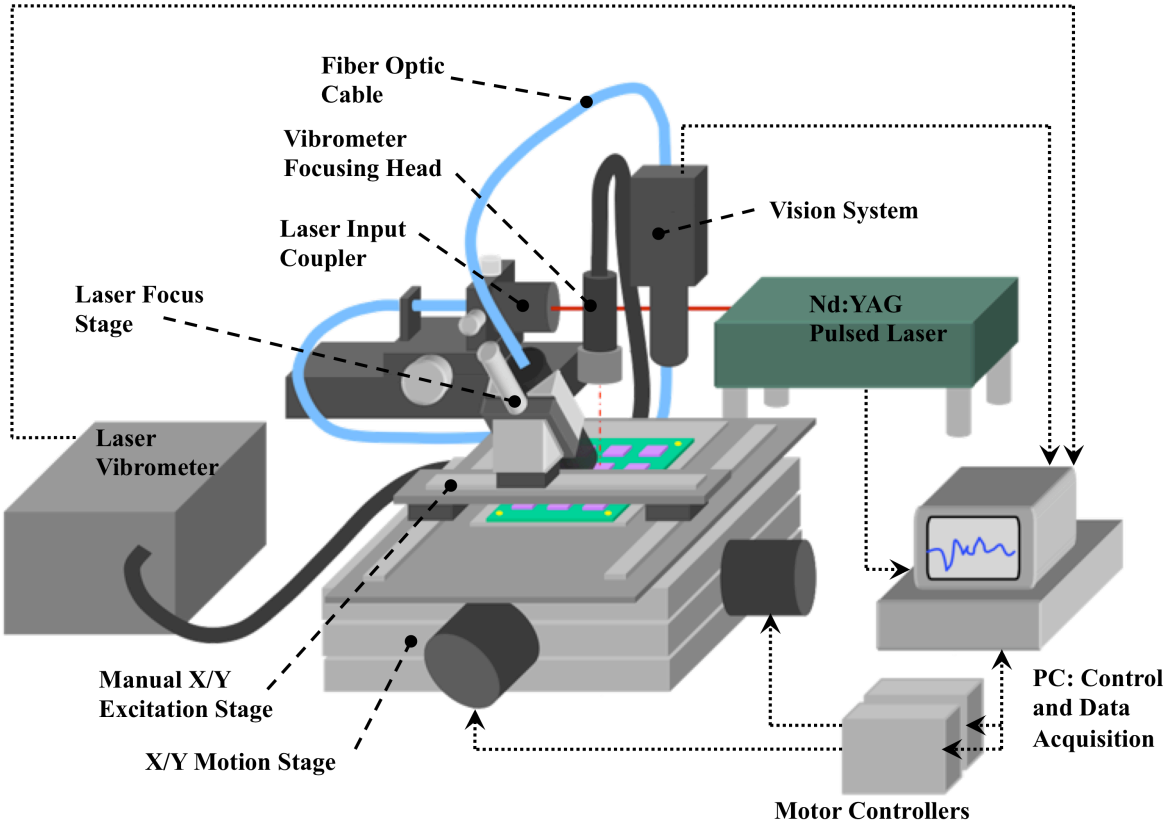

Figure 2.1: Original nondestructive inspection prototype.

The system has a Nd:YAG pulsed laser that is directed at a laser input coupler connected to a fiber optic cable that allows the laser spot to be positioned and focused by the laser focusing stage. As the laser induces vibration in the IC chip, a laser vibrometer measures the out of plane vibration. The vibrometer has a fiber optic cable ending with a focusing head held rigidly above the motion stage. Measuring the vibration with a laser has many advantages over other sensor types. One significant advantage is that the measurement

method does not disturb the surface vibration while providing a flat broadband frequency response and fine sub-nanometer resolution with a single sensor.[11] By limiting the bandwidth of the vibrometer to a range of 25kHz to 2 MHz, the noise level is able to be reduced to approximately 0.07 nm.[12] Signal processing is utilized to eliminate low frequencies, eliminating the need for extensive environmental vibrational isolation for the vibrometer.[13] The vibrometer used in this work is a laser heterodyne interferometer, which uses the Doppler affect to measure displacement through changes in frequency shift.[14] A vision system is used to determine the exact location and orientation of the PCB on the X/Y motion stage. The motion stage controls the position of the IC relative to the laser vibrometer. A computer controls the motion stage, vibrometer, and pulsed laser.

Prototype Limitations

There were some limitations to the original prototype; the first of which was that it was not fully automated. Many of the inspection subsystem's components were automated, but were all controlled using their own custom software. There was no single interface to control the entire prototype.

One subsystem that was not automated at all was the laser vibrometer. For the original inspection prototype, the vibrometer was adjusted manually by rotating the threaded 16mm aperture lens-housing of the focusing head.[10] When the signal strength was seen to be poor by viewing the signal on an oscilloscope, the operator would manually adjust the focal length by rotating the lens-housing to attempt to improve the signal strength. The manual adjustment was very time consuming and delicate. Lightly touching the focusing head was enough to change a poor signal into a very strong one. This meant that when the operator removed his/her hand from the focusing head after finding a strong signal, the signal would often drop back to a lower signal intensity strength. This required the operator to make an adjustment, let go, and see how the change affected the signal. This process might have to be repeated several times before finding suitable signal intensity strength. This also meant that the quality of the signal that was being recorded often varied greatly with the skill and patience of the operator. This limitation of the vibrometer facilitated the need for a fully automated system to

maintain the signal intensity strength that was completely hands-free, which would improve the throughput and the repeatability of the vibrational data acquired by the vibrometer. The lack of customization available in current commercial autofocusing vibrometers and their relative slow refocusing time, created the need for the system that was developed in this thesis.

CHAPTER 3

AUTOMATED VIBROMETER SIGNAL INTENSITY ADJUSTMENT SYSTEM

System Hardware

Overview of Hardware

The automated signal intensity adjustment system was designed to be a stand-alone system with its basic components shown in Figure 3.1. The system consists of a laser vibrometer used on the original measurement system. The vibrometer is attached to a motorized linear actuator with a telescoping mount that gives adaptability to where the vibrometer head is located. This mounting configuration was chosen to allow the signal intensity adjustment system to be integrated into the existing inspection prototype with minimal alterations. This was required to allow the inspection prototype to be used by other members of the research group to capture data while the signal intensity adjustment system was being integrated. The positioning of the vibrometer head at the end of a cantilever beam does make the system more prone to vibration, but was necessary for the requirements mentioned above. The linear actuator controls the standoff distance from the vibrometer head and the surface of the chip package being inspected. This control of standoff distance is how signal intensity strength is adjusted, along with the positioning of the IC by the X-Y stage. The signal intensity adjustment system is in green and the existing components of the original measurement system are in gray.

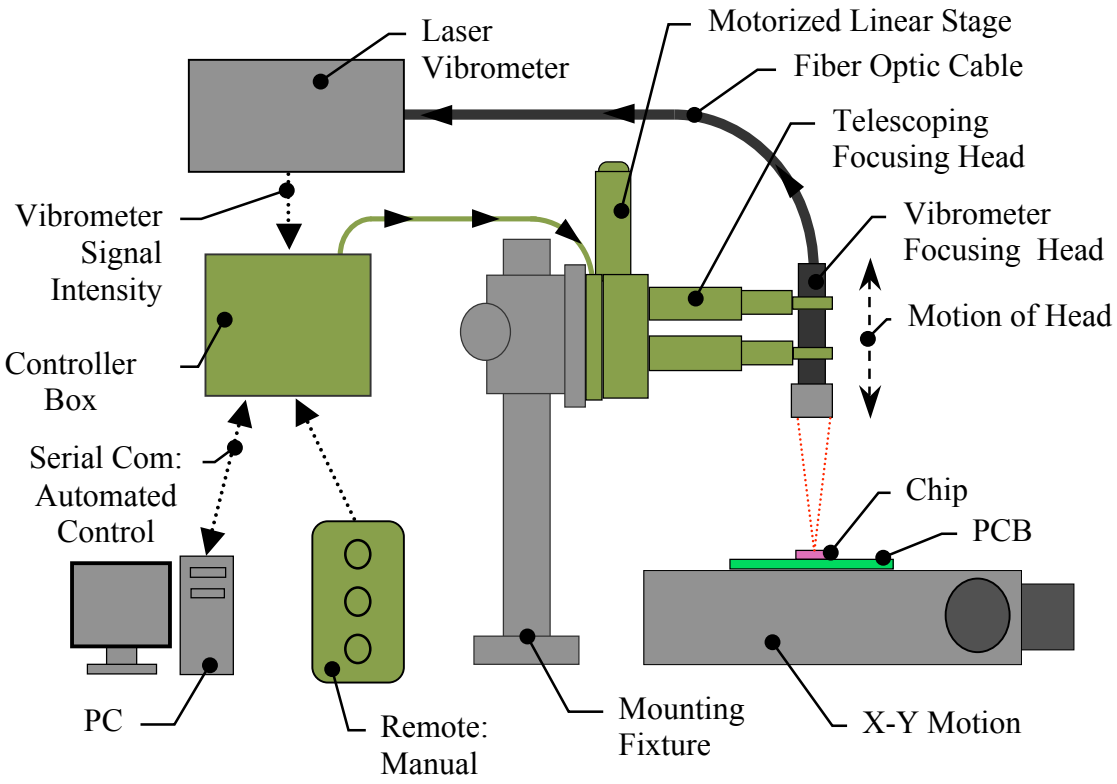

Figure 3.1: Configuration of automated signal intensity adjustment system.

The controller box, shown in Figure 3.2, contains a power supply, microcontroller, and stepper motor driver for the linear actuator. The controller box takes the vibrometer signal intensity, which has been correlated to inspection resolution[10], as an input, and outputs the desired motor position. An algorithm was developed to reduce the time needed to fine a strong signal intensity strength, while maintaining accuracy and repeatability. The system can be controlled either by a remote with buttons for manual input or through a serial communication port to a personal computer (PC) for automated control through software like MatLab.

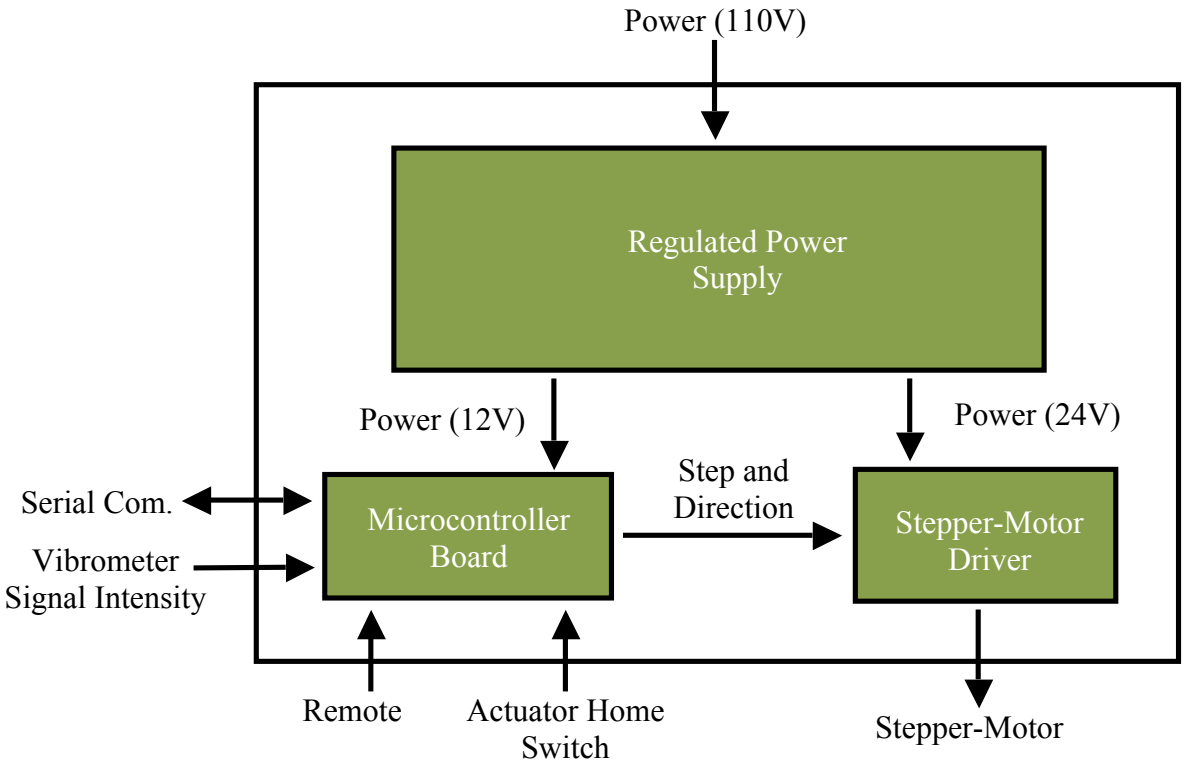

Figure 3.2: Diagram of controller box showing power and information flow.

Linear Actuator

The motorized linear actuator controls the standoff distance from the vibrometer focusing head and the chip package surface that is being inspected. The actuator, shown in Figure 3.3, was manufactured by Melles Griot and its part number is 07 ELC 204. The actuator is made up of a 65X65 mm aluminum ball-bearing stage part number 07 TLC 224 and a stepper-motor linear drive part number 07 EAS 503. The manufacture's specification claims that the actuator has a maximum speed of 4 mm/sec, a travel of 13 mm (0.5 inch), a load capacity of 4 kg (8.8 lb), a positioning resolution of 0.5 µm (when microsteping), and bidirectional repeatability of <4 µm. The stepper-motor is 2-phase with 200 steps per revolution. The lead screw has a pitch of 1 mm. The stepper-motor linear drive also contains an internal "home" switch for the completely retracted position and a knob at the end of the drive for manual positioning, if desired.

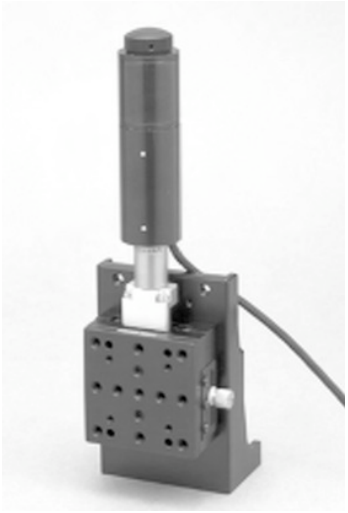

Figure 3.3: Linear actuator for positioning the vibrometer focusing head.

A test was conducted to find the maximum speed the actuator could be run without missing steps and losing its repeatability. This test consisted of the actuator moving to the home position, then to a set of positions, which required the actuator to change direction quickly and move both long and short distances. At the end of the test, the actuator would return back to the home position, keeping track of how many steps it took to reach home. This number was compared to the theoretical number of steps it would need to get home. If steps were missed, the two numbers would not match and an error was detected. The maximum step pulse rate at which no steps were lost was found to be 3.125 kHz. This maximum step pulse rate gave a max operating speed of 1.56 mm/sec for the actuator.

Controller Box

The controller box contains all the electronics for the autofocusing system. As seen in Figure 3.2, the controller box consists of a regulated power supply, stepper-motor driver, and microcontroller.

The regulated power supply shown in Figure 3.4, is made by Sola model number SLD-12-1818-12T. The voltage output of the power supply is +12 VDC at 1.8 A and -12 VDC at 1.8 A. The +12 and -12 VDC are tied together to deliver 24 VDC at 1.8 A to the

stepper-motor driver, and +12 VDC is supplied to the microcontroller board which was then regulated down to 5 VDC for the microcontroller.

Figure 3.4: Regulated power supply for controller box.

The stepper-motor driver, shown in Figure 3.5, is made by Geckodrive model number G251. The drive operates from 15-50 VDC with a max phase current of 3.5 A. The step pulse rate range for the drive is 0-300 kHz. The resolution of the drive is 10 microsteps per full step. When combined with the stepper-motor's resolution discussed earlier, there were 2000 microsteps per revolution. With a lead screw that has a pitch of 1 mm per revolution, the positioning resolution of 0.5 μm per step was achieved by the stage. The inputs to the drive are step pulse, direction, and disable.

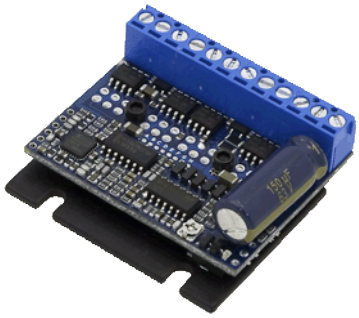

Figure 3.5: Stepper-motor driver to control the linear actuator.

The microcontroller board is a custom development board, which consists of a 5 VDC voltage regulator, PIC microcontroller, serial communication chip, and an assortment of switches, LEDs, and pins for rapid development. The microcontroller used is the Microchip PIC18F4523. This 8-bit microcontroller runs at 20 MHz. The primary

reason for using this particular microcontroller is that it has a 12-bit analog-to-digital converter (ADC) that is configured for a range of 0-5 V resulting in a resolution of 1.22 mV per bit and a sampling rate of 6.25 kHz. The vibrometer signal intensity, which is a direct current (DC) signal, is connected to the microcontroller's ADC. Both the remote and the actuator home switch are connected to input-output (I/O) pins of the microcontroller, which are configured as inputs. The stepper-motor drive's step pulse and direction are connected to I/O pins configured as outputs.

The housing of the autofocusing controller is an aluminum sheet metal project box with all the components shown in Figure 3.2 mounted to the bottom plate. Figure 3.6 shows the back plate of the autofocusing controller box, which contains all the panel-mounted power, inputs, and outputs.

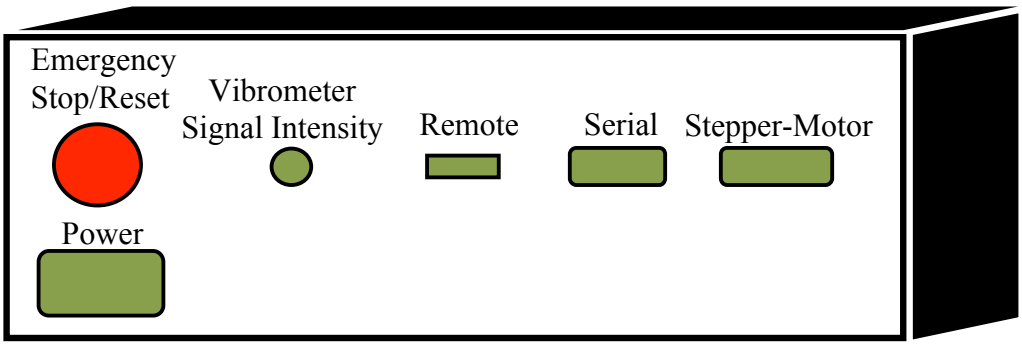

Figure 3.6: Controller box back panel layout.

The power is a standard IEC C14 socket, which takes an IEC C13 plug (standard computer plug). The emergency stop/reset button is a twist-to-release type switch to stop the system in an emergency situation or just to reset the system. The vibrometer signal intensity is a BNC connector. The remote is a USB socket (not true USB) that the remote module plugs into. The serial is a DB-9 connector that is for RS 232 serial communication at a baudrate of 57600. The stepper-motor plugs into a DB-15 connector that contains the power for the motor and the home switch in one cable.

Vibration Reduction With Input Shaping

As seen in Figure 3.1, the vibrometer focusing head is mounted on the end of two telescoping posts. This was done to integrate the autofocusing system into the existing measurement system without reconfiguring the entire original system discussed in the "Overview of Hardware" section above. The result was that the vibrometer head that was attached to the end of a cantilever beam was more susceptible to vibration than if attached closer to the linear actuator. The linear actuator was moved a set distance and at the end of the motion, the signal intensity of the vibrometer was recorded to observe any oscillation in the signal the motion had produced. As the vibrometer head vibrated, it would change the signal intensity producing a measurement of the vibration. The test procedure used was as follows: The height (number of steps from the home position) at which a strong signal was found was recorded manually; the actuator would move the focusing head to a set distance away from the previously recorded location. The system would stand at rest for 10 seconds, which was experimentally found to be a sufficient amount of time to allow all other vibrations from the system to die out; the actuator would then move the focusing head to the next previously recorded location, and the ADC would immediately start saving the signal intensity values into the microcontroller's memory. After capturing all the data, it was then sent through serial to a PC for processing. This test was conducted using a flip chip test vehicle, and the response in the time domain can be seen in Figure 3.7.

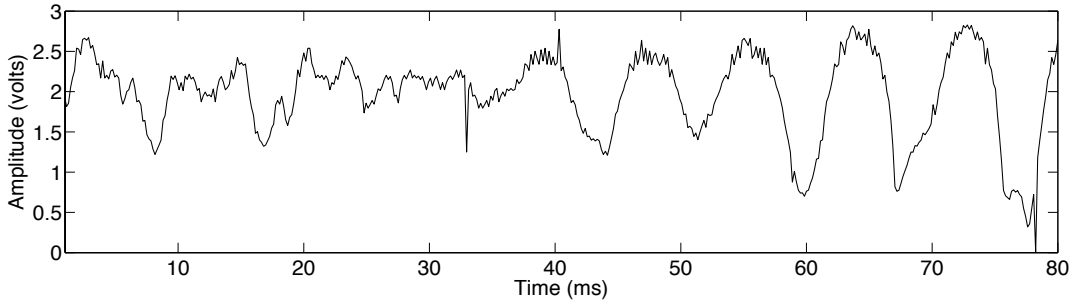

Figure 3.7: Amplitude of vibrometer signal intensity after step response.

As seen, there was a large amount of oscillation in the signal intensity strength after the step response. The Fast Fourier Transform (FFT) was performed on this data and the

results are shown in Figure 3.8. The red arrows indicate the resonant frequency of the system at 120 Hz .

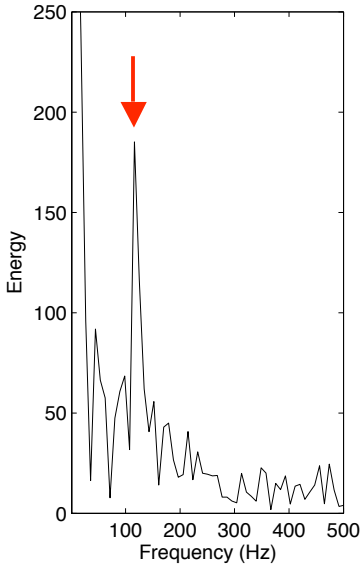

Figure 3.8: FFT of vibrational response of system.

This shows that the resonance frequency of the system is approximately 120 Hz. The natural frequencies of the mounting post and the telescoping mounts were calculated with Equation 3.1.

$$\omega_n = \sqrt{\frac{k}{m}} \quad \text{(Hz)} \tag{3.1}$$

Were k is stiffness of the cantilever beam, and m is the mass of the beam. The stiffness k is shown in Equation 3.2

$$k = \frac{3EI}{L^3} \quad \text{(N/m)} \tag{3.2}$$

Were E is Young's Modulus of Elasticity, I is the bending moment of inertia, and L is the length of the cantilever beam. The stiffness of the mounting post was calculated to be 748,000 N/m with Equation 3.2 and its natural frequency was calculated to be 5260 Hz

with Equation 3.1 (with the values of E = 70 GPa, I = 7.82x10^{-8} m^3, L = 0.28 m, and m = 0.397 kg). The telescoping mount was modeled as two springs in parallel and had a calculated stiffness of 2,751,000 N/m and a natural frequency of 4160 Hz (with the values of E = 70 GPa, I = 1.20x10^{-9} m^3, L = 0.15 m, and m = 0.159 kg). These calculations showed that these portions of the system were sufficiently stiff and not the cause of the 120 Hz oscillation in the signal intensity seen in Figure 3.8. Therefore, the vibration was most likely the result of the flexibility in the linear actuator stage that was amplified by the cantilever beam. This assessment of the flexibility in the system was confirmed by observing deflection in the stage when applying light pressure to the end of the telescoping mount. This could be eliminated in future designs by using a stiffer stage and mounting the vibrometer as close to the stage as possible. With the constraints to the system previously described, resulting in the need of the cantilever beam, the method of reducing the vibration was chosen to be input shaping. Input shaping was chosen over other control methods like PID, because there was no direct feedback of the position of the end of the cantilever beam. The oscillation seen in Figure 3.7 is of the signal intensity strength, which is greatly affected by the vibration of the beam but not a true measurement of position that would be needed to implement control methods like PID in a reliable manner. This lack of true feedback is why input shaping was chosen, which is a method that does not require feedback to reduce vibration.

Introduction to Input Shaping

Input shaping is not a feedback control method; it requires that an estimate of the system resonant frequencies be known. Input shaping reduces vibration in the system by shaping the input command in a way that the vibratory modes of the system are canceled out[15]. This is achieved by convolving the input command with a sequence of impulses. This method is shown in Figure 3.9.

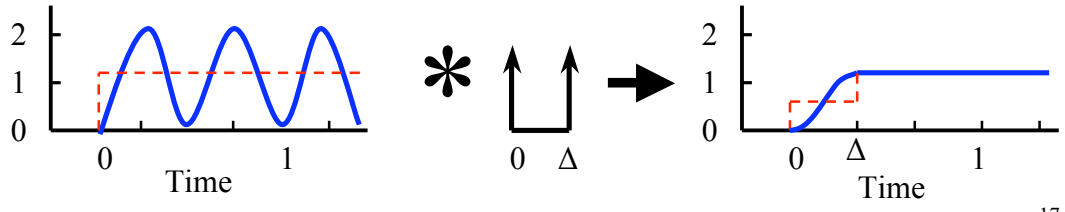

Figure 3.9: Input shaping control method, --- input command, – system response.[17]

To move a system that has one primary resonant frequency with input shaping to a set velocity, the controller would drive the system at half the speed for half the period of the resonant frequency and then change the velocity to the full desired speed from there on. These two step-impulses would excite two instances of the resonant frequency at the same magnitude that were 180° out of phase, which would cancel each other out.

Implementation In Signal Intensity Adjustment System

To implement input shaping in the system, the code was modified to include the input shaped acceleration when starting and ending a move. Using 120 Hz as the estimate of the resonant frequency of the system, which is found in Figure 3.8, the time needed to run half the speed in half the period was 4.16 ms, which corresponds to 6 steps of the stepper-motor when the full speed step rate was 3.125 kHz. Whenever a specific number of steps of the stepper motor are used in the description of input shaping below, they are specific to the hardware used for the signal intensity adjustment system and not to input shaping in general. With input shaping implemented, the step response of the signal intensity adjustment system was again found and is shown in Figure 3.10. Flip chips were used as test samples for all of the tests concerning input shaping.

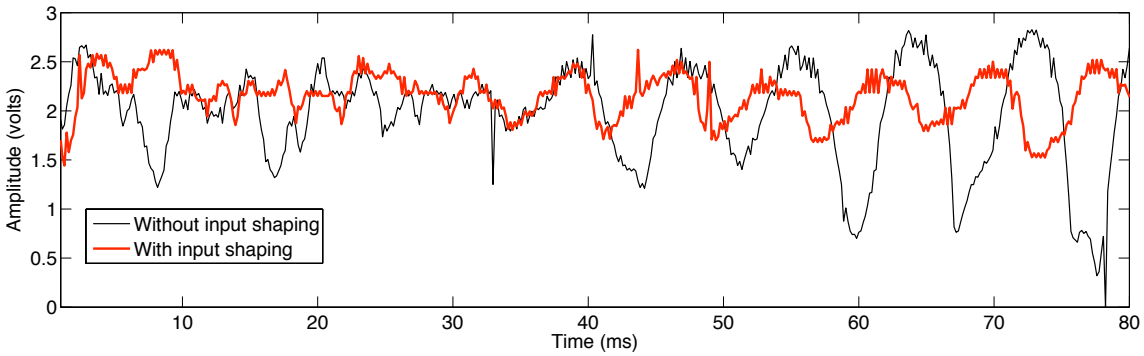

Figure 3.10: Amplitude of the vibrometer signal intensity with and without input shaping.

The peak-to-peak amplitude of the step response with input shaping can be seen to have been reduced by as much as half compared to the step response amplitude without input shaping. Figure 3.11 shows the FFT of the step response without and with input shaping

implemented. The red arrows indicate the resonant frequency of the system at 120 Hz, while the blue arrows indicate signal intensity noise of vibrometer at 60 Hz.

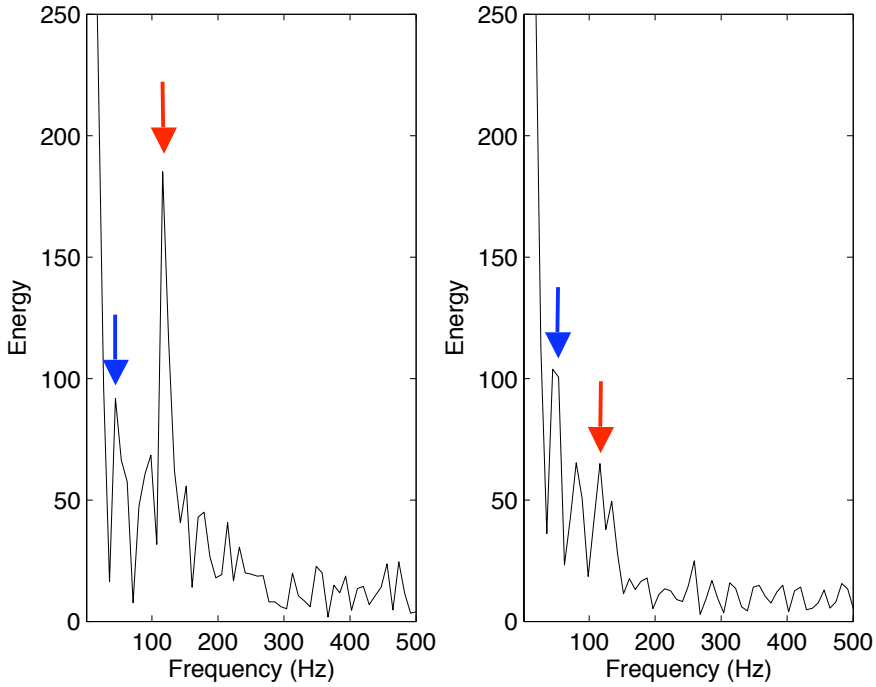

(a) Without input shaping (b) With input shaping

Figure 3.11: FFT of response of system with (a) and without (b) input shaping.

As seen in Figure 3.11 (b), the input shaping reduces the energy of the resonant frequency at 120 Hz (red arrow). The remaining peak is at approximately 60 Hz (blue arrow), which is also seen in Figure 3.10, and is an electrical noise that is inherent to the vibrometer signal intensity output. A lowpass active filter was designed and tested to eliminate the 60 Hz noise. The filter was not used due to its large lag time measured to be 8 ms.

As seen in Figure 3.9, there was a limitation on when the input shaping could be implemented. There was a half period ramp-up time and a half period ramp-down time that was required when making a move. Theoretically, this means that the input shaping would only work when the move required more than 12 steps (6 μm) of the stepper-motor. Figure 3.12 shows the FFT of the step response of the system after a step input of length 13-19 (6.5-9.5 μm) steps in 1-step (0.5 μm) increments. The red circles show the presence of the resonant frequency at 120 Hz.

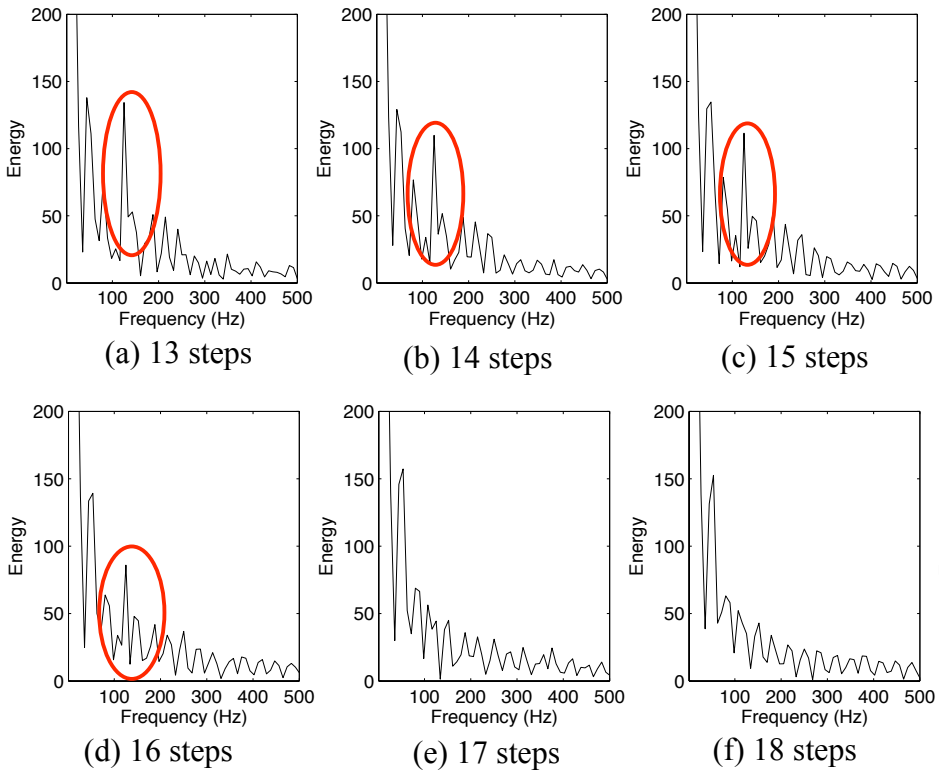

Figure 3.12: FFT of step response of system after a step input of 13-18 steps in length.

This shows that the resonant frequency is not cancelled substantially after the theoretical 12 steps (6 μm), but it is at 17 steps (8.5 μm) that the resonant frequency is substantially canceled out as seen in Figure 3.12 (e). This difference from the theoretical minimum distance can be accounted for in the inability of the stepper motor to achieve the exact ramping period from the fact that it can only move in steps of discrete distance depending on the resolution of the motor and driver used. This test shows that the distance traveled has to be longer than 17 steps (8.5 μm), or duration of motion of more that 9.3 ms, before the input shaping would be effective.

The majority of the motion of the automated signal intensity adjustment system is made up of both long movements, which are greater than 100 steps (50 μm), and very short movements of 2 steps (1 μm). The input shaping would effectively suppress the vibrations of the long movements. A test similar to that described in Figure 3.12 was conducted to determine the size of the step input needed to excite the resonant frequency. Figure 3.13 shows the FFT of the step response of the system after a step input of length

1-8 steps (0.5-4 µm) in 1-step (0.5 µm) increments. The red circles show the presence of the resonant frequency at 120 Hz.

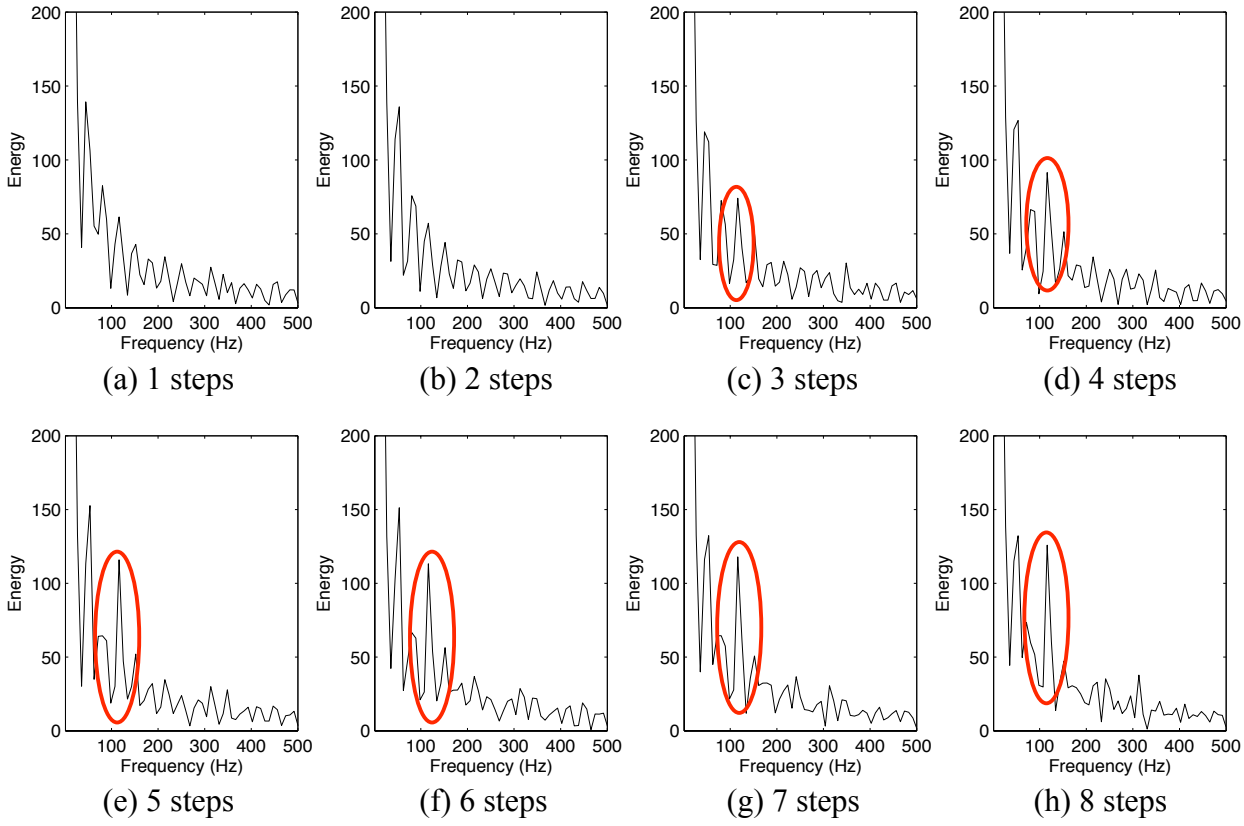

Figure 3.13: FFT of step response of system after a step input of 1-8 steps in length.

This test shows that the resonant frequency of 120 Hz required a step input of 3 steps (1.5 µm) or greater to be excited. As seen in Figure 3.13 (c), the resonant frequency first appears at 3 steps and increases in strength until it reaches 5 steps (2.5 µm) Figure 3.13 (e). The results from Figure 3.12 and Figure 3.13 show that before 3 steps (1.5 µm) no input shaping is needed, and after 16 steps (8.5 µm) input shaping is fully developed reducing the oscillation of the signal intensity strength.

Signal Intensity Adjustment Algorithm

The signal intensity adjustment algorithm has to accomplish two main purposes. The first purpose is to increase the repeatability and ease of use of the original inspection prototype. This requires that the system be able to operate for a wide variety of

inspection configurations. Different configurations involve different thicknesses of boards, chip layouts, and the need to adjust a single time or multiple times for multiple measurements. Commands to adjust by the operator and easy control over the algorithm's parameters are also needed to allow the system to be quickly adapted to changing research needs. The second purpose is that the signal intensity adjustment algorithm must accommodate the ability to be configured for a specific inspection configuration to demonstrate the feasibility of the measurement system in an online inspection capacity. This would reduce the flexibility of the system for other inspection configurations but reduce the inspection time for that specific configuration. This would require that a greater amount of information be supplied to the signal intensity adjustment algorithm specific to that configuration.

Overview of Signal Intensity Adjustment Algorithm

The signal intensity adjustment algorithm was based on an assumption that when the focusing head was out of focus, the signal intensity strength would be very low. The strength of the signal intensity input would then increase to a peak and then decrease back to a very low strength. The peak of the curve generated by this sweep would then give the optimal standoff height. An initial study was conducted to learn how the signal intensity strength changed during a scan described above to validate this assumption. Figure 3.14 shows eight scans of different chip packages made by the signal intensity adjustment system, four using a BGA chip and four using a flip chip, all at a standoff height resolution of 4 steps (2 μm). These plots show a profile of how the signal intensity changes with respect to standoff height with a fixed focal length.

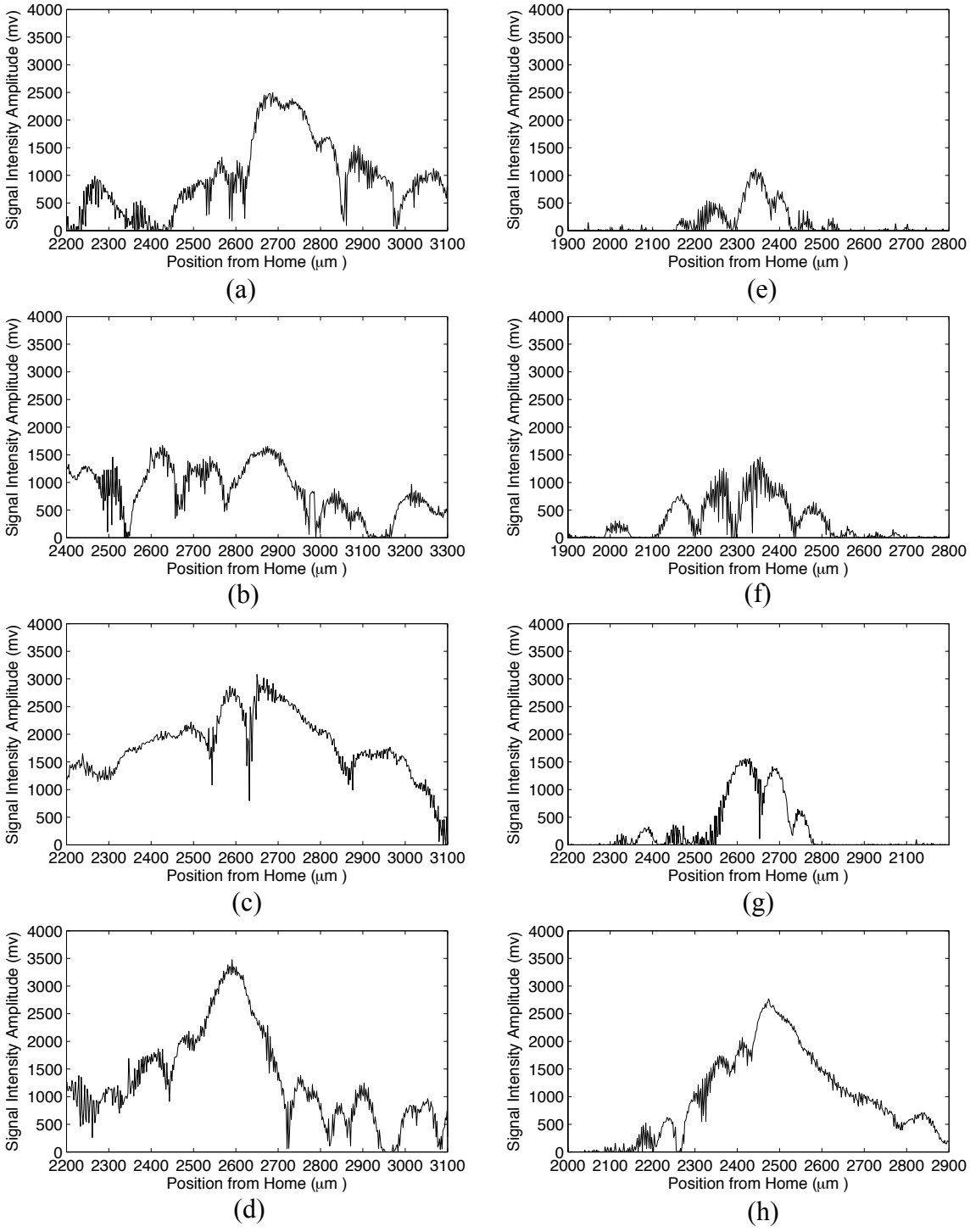

Figure 3.14: Signal intensity profiles of 4 flip chip packages (a)-(d) and 4 BGA chip packages (e)-(h).

This test was performed by first moving the focusing head to the home position of the linear actuator, which was the lowest standoff height. The focusing head then moved up 2 steps (1 μm) and then took 10 samples of the signal intensity strength with the microcontroller's ADC at a sampling rate of 6.25 kHz. The system would then repeat this move-and-sample routine until reaching the travel height of 10,000 steps (5 mm), which was far above the optimal focus location for most applications. These 10 samples where then averaged to produce the curves in Figure 3.14. The signal strength scale (Y) was held constant for comparison purposes while the standoff height scale (X) was shifted to window the peak. The shift in the standoff height represents the difference in the optimal focusing height, which was seen to differ from chip package to chip package. A more in-depth study of the standoff height variation will be discussed further in this section. Figure 3.15 shows an example of the full scan data of a flip chip with a standoff height resolution of 20 steps (10 μm).

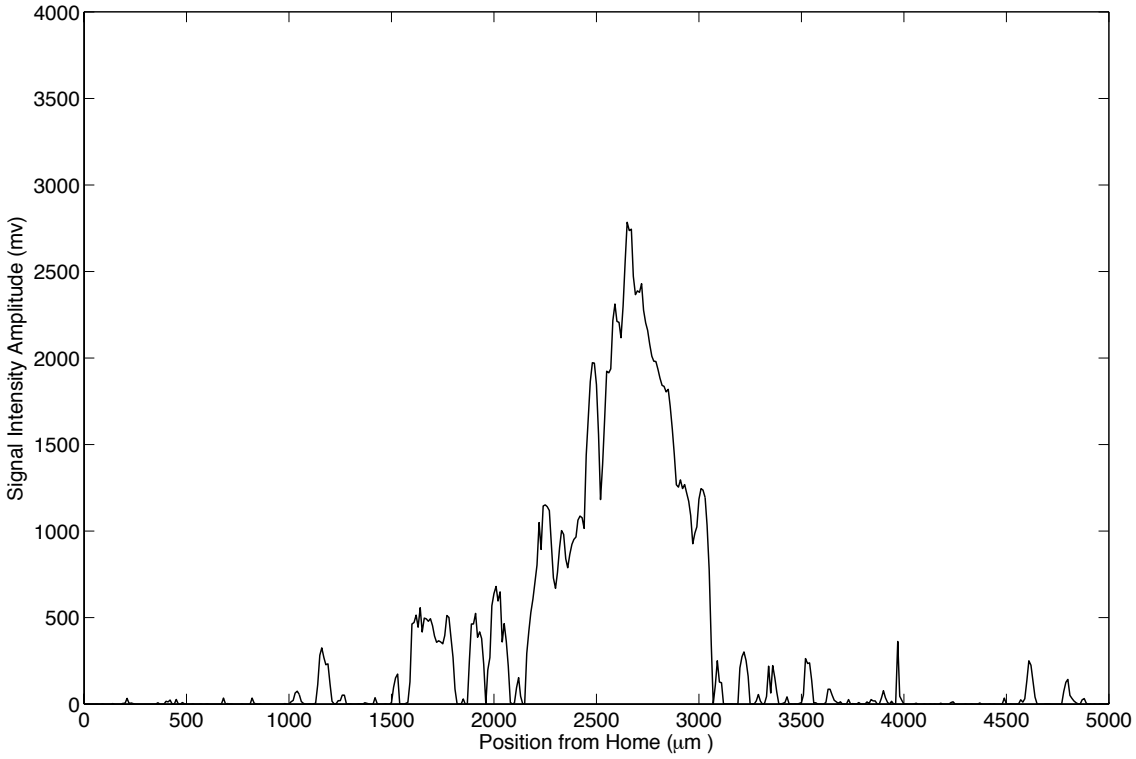

Figure 3.15: Full signal intensity strength profile of flip chip.

As seen clearly in Figure 3.15, the initial assumption that the scan would produce a bell-curve shape profile was validated.

Overall, the amplitudes of the BGA's peaks were lower than that of the flip chips, which correspond to the smooth reflective surface of the flip chip compared to the plastic textured finish of the BGA's surface.[16] However, Figure 3.14 (h) is a scan of a BGA package with the laser focused onto text printed on the package's surface, which was more reflective than other areas of the package, producing a larger peak than typical of BGA packages.

Figure 3.14 clearly shows a large variability in the peak amplitude and the specific shape of the curve. Most notably, the presence of large local maximums near the global maximum peak made the detection of the global maximum problematic. An attempt was made to create a smart algorithm to detect the global maximum peak. The reliability of the algorithm was very low due to the unpredictable specific shape and magnitude of the global maximum. Due to this, the method chosen to find the global maximum was to scan over a region and then return to the location with the highest amplitude. This method is slower than other peak-finding algorithms, but has the highest reliability of finding the global maximum.

There are two primary portions of the signal intensity adjustment algorithm, the initial adjustment and readjustment. The initial adjustment allows the adjustment system to find the proper standoff height with no prior knowledge of the chip package geometry. The readjustment algorithm uses the previous global maximum as the starting point for finding the next global maximum.

Initial Adjustment Algorithm

There are two stages to the initial adjustment algorithm. First, a fast, inaccurate full scan is conducted to find a general starting point; second, a slower, more precise, narrower scan for the actual optimal standoff height is performed. This is desirable for rapid testing of different sized chip packages and circuit boards. There is no need for any hand adjustments of the automated signal intensity strength adjustment system at any time. Figure 3.16 shows a diagram of how the focusing head moves as the scan is

progressing through the initial adjustment routine, from an unknown starting location to the standoff height that produces to strongest signal intensity found. The red lines in the diagram are not showing the specific velocity of the focusing head, but are to be used to understand the general concept of the motion.

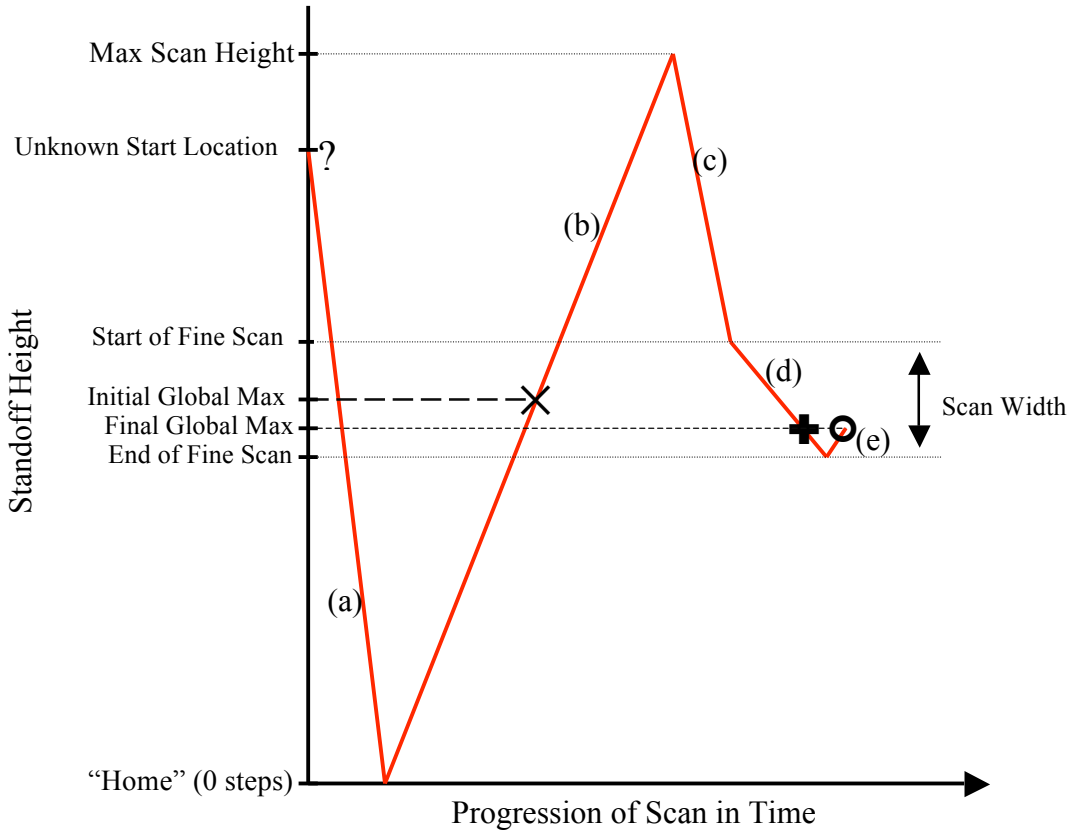

Figure 3.16: Diagram of the initial adjustment routine.

In Figure 3.16 the line (a) represents the linear actuator moving from an unknown starting location to the home position at full speed (1.56 mm/s). This is because the linear actuator is driven by a stepper motor with no positional feedback. When the system is started, the actuator needs to have a repeatable reference point from which the dead reckoning is based. Line (b) shows the system scanning from the home position to the max scan height. The speed with which this is done is determined by the number of steps between data points, standoff height resolution, and the number of signal intensity strength samples averaged at each data point, and this will be discussed below. The purpose of this scan is to quickly find a general starting point to look for the more precise

final global maximum. As the system scans up, the location (in steps) of the maximum value of the signal intensity input to the ADC is recorded. Line (c) shows the focusing head moving back down to the start position of the fine scan at full speed. The start location of the fine scan is the initial global maximum plus half of the scan width. The scan width will be discussed in the readjustment algorithm section. This centers the fine scan on the initial guess of the global maximum. Line (d) shows the focusing head scanning down to the end position of the fine scan. This scan is slower than that conducted by line (b) with a finer standoff height resolution and larger number of samples of the signal intensity strength averaged at each data point. Similar to the scan by line (b), the location of the maximum signal intensity is recorded. Finally, line (e) shows the focusing head moving back up at full speed to the precise global maximum. Both the scan width and the parameters of the fine scan will be discussed in the next section because they are essentially what make up the readjustment algorithm.

For the initial scan, the two parameters are the number of steps between each data point (standoff height resolution) and the number of samples of the signal intensity strength averaged at each location. These two parameters control the speed of the scan and the accuracy of the initial scan to find the global maximum of the signal intensity strength profile. The time is the primary concern because the accuracy can be accounted for in the fine scan later.

A test was conducted to determine the standoff height resolution and number of samples of the signal intensity strength that were averaged at each data point by iterating through 100 permutations of standoff height resolution and number of samples averaged at each data point, both going from 1-19 in 2 step increments. For each permutation, the initial adjustment routine was conducted at the given parameters; the maximum signal intensity strength that was found and its standoff height were recorded. This scan was performed 10 times for each permutation. This test was conducted 6 times at 3 different locations on a flip chip and at 3 different locations on a BGA chip. Overall, 6000 scans were conducted.

Figure 3.17 shows the contour plot of the time needed to conduct an initial adjustment routine (full scan) of each permutation in seconds.

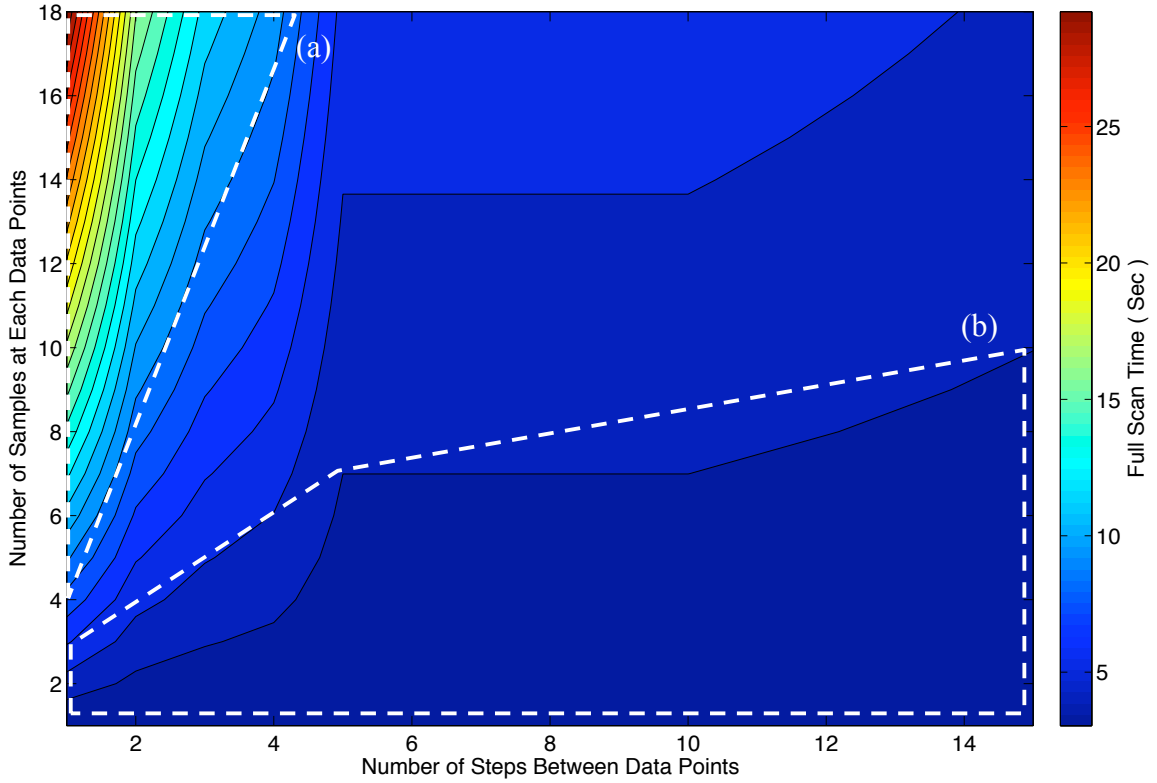

Figure 3.17: Contour plot of the time needed to conduct a full scan: (a) shows the slow region, (b) shows the fast region

As seen in Figure 3.17 region (a), to conduct a full scan at high resolution of both standoff height and number of samples averaged takes a relatively large amount of time, which is an obvious result. Region (b) shows the permutations of the full scan that have the desirable shorter scan time.

Figure 3.18 shows the contour plot of the error of each permutation's optimum standoff height in steps. The error was calculated by finding the absolute difference between the permutation's global maximum and a reference global maximum. In this case, the reference global maximum was found by conducting 20 full scans at the given location with the best resolution (1 step, 0.5 μm) and 200 samples of the signal intensity strength averaged at each data point. The average of these 20 scans produced the reference global maximum. A reference global maximum was found for each different location that was scanned.

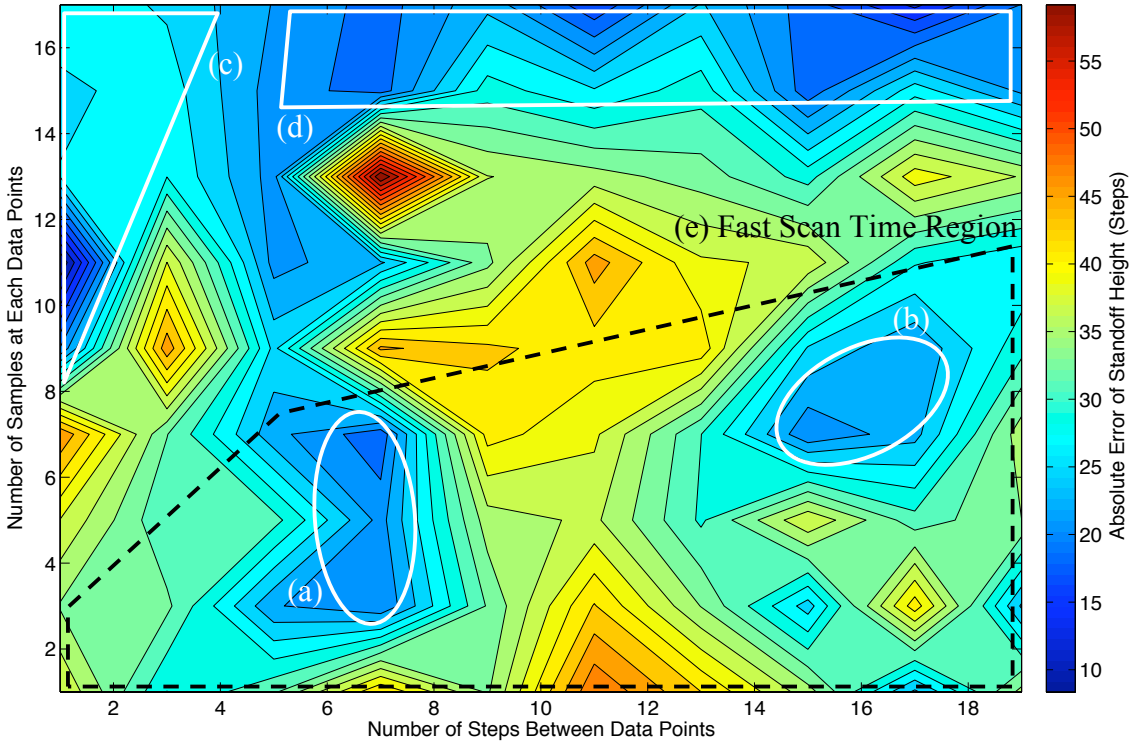

Figure 3.18: Error of each permutation's optimum standoff height (global maximum). (a) – (d) are calling out regions of interest in white. (e) shows the desired scan time region in black.

As seen in the color bar, the darkest blue areas represent permutations with low error and are most desirable. The lowest error was found in region (c), but as seen in Figure 3.17 (a), this corresponds to a very slow scan time. Region (d) has low error, but is not in the desired fast scan region (e) found from Figure 3.17 (b). Figure 3.18 (a) and (b) both have fairly low error and are in the region (e) making them potential candidates. To determine which region is most desirable, the standard deviations of the permutations were investigated.

Figure 3.19 shows the contour plot of the average standard deviation of each permutation's global maximum in steps. For each of the permutations at a given location, the standard deviation of the offset height for the 10 scans was calculated. Because the data at each location is independent of each other, the average of the 6 standard deviations can be calculated for each permutation giving overall standard deviations.

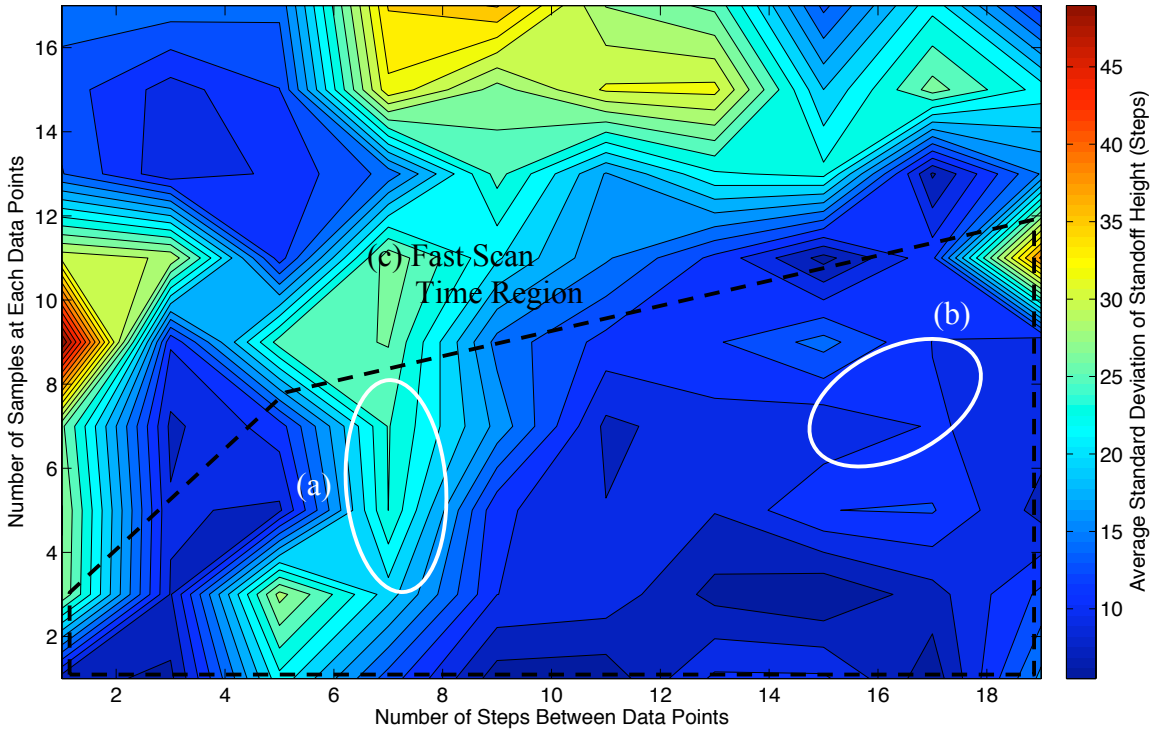

Figure 3.19: Standard deviation of each permutation's standoff height (global maximum). (a) and (b) call out regions of interest in white. (c) shows the desired scan time region in black.

Figure 3.19 clearly shows that between regions (a) and (b), region (b) has the lowest standard deviation giving the best permutation for the initial scan. This gives the parameters to be 15 steps (7.5 μm) between data points (standoff height resolution) and 7 samples of the signal intensity strength averaged at each data point, Figure 3.19 (b). These parameters produce an average error of 20.8 steps (10.4 μm), with a standard deviation of 9.3 steps (4.7 μm).

With these parameters of the standoff height resolution of 15 steps (7.5 μm) and 7 samples averaged at each data point for the initial scan, and a max scan height of 10,000 steps (5,000 μm), which is the range that includes all the test samples currently used by this nondestructive inspection prototype, along with the fine scan parameters (which will be discussed in the next section) of a standoff height resolution of 2 steps (1 μm), 25 samples averaged at each data point, and a scan width of 600 steps (300 μm), the average initial adjustment time was found to be 8.9 sec. This time will vary slightly on how far the focusing head has to move from the end of the fine scan to where the final global maximum was found, and how far the focusing head has to move from the unknown

starting location to the home position.

Readjustment Algorithm

This algorithm was based on the assumption that the location on the IC being inspected was fairly close to the previous inspection location and at the same general height. With this assumption, the center point of the fine scan can be the previous global maximum instead of the initial global maximum found by the inaccurate initial scan. Figure 3.20 shows a diagram of how the focusing head moves as the scan is progressing through the readjustment routine, from the standoff height of the previous global maximum to the standoff height of the new global maximum of the signal intensity profile. The red lines in the diagram are not showing the specific velocity of the focusing head, but are to be used to understand the general concept of the motion.

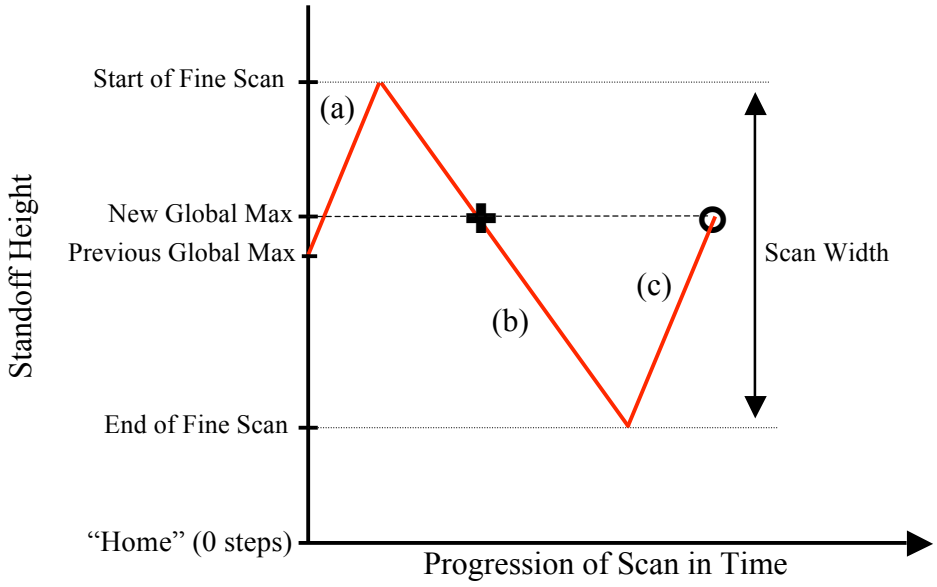

Figure 3.20: Diagram of readjustment routine.

Figure 3.20 shows a routine that is very similar to that shown in Figure 3.16. Line (a) shows the focusing head moving up at full speed to half of the scan width to the starting position of the precise scan. The head then moves down, shown by line (b), at a speed governed by the number of steps between data points (standoff height resolution) and the

number of samples of the signal intensity strength averaged at each data point. When the fine scan is finished, the focusing head then moves back up at full speed to the location where the highest amplitude of the signal intensity strength of the vibrometer was found during the fine scan. Like in the initial scan, the three main parameters controlling accuracy and scan time were standoff height resolution, the number of samples averaged at each data point, and the scan width. Each of these parameters will be discussed in detail below.

From Figure 3.13, there are only two high-standoff height resolution choices for the number of steps between data points that will not induce a resonance in the system, which are 1 and 2 steps (0.5 and 1 μm). From Figure 3.14 it can be seen that the global maximum, besides the noise, is typically at the peak of a smooth curve, which makes the accuracy of the location of the global maximum less sensitive to small reductions in resolution. The readjustment time with a standoff height resolution of 2 steps (1 μm) will be half the time with a standoff height resolution of 1 step (0.5 μm), due to the fact that only half as many data points are captured. To achieve a shorter readjustment time with a very small reduction in accuracy, a standoff height resolution of 2 steps (1 μm) was chosen.

To determine the number of samples to be averaged at each data point, a test was conducted to find how the standoff height of the global maximum of the signal intensity profile found in the fine scan was affected by the number of samples averaged at each data point. Figure 3.21 shows the results of this test for 4 different locations on a flip chip. At each data point in Figure 3.21, error bars were included. These give the one standard deviation variation of the average at that point. The bold lines give a reference value for the long-term average of the standoff height of the global maximum. This reference was calculated by taking the average of the data points after the curve was seen to level out at 160 samples (the green arrow in Figure 3.21).

The test consisted of returning to the home position and then running an initial scan. The focusing head then would move half the scan width, which was 600 steps, and then with a resolution of 2 steps (1 μm) take data with the specified number of samples of the signal intensity strength averaged at each data point. When the scan was complete, the standoff height of the global maximum was recorded and the focusing head would

return to the start position of the fine scan and rescan. The number of samples averaged at each data point that were iterated through was 5 through 250 samples in 5 sample increments. For each different number of samples, the scan was repeated 10 times. This resulted in 2500 scans for the standoff height of the global maximum per location. The four locations tested on a flip chip produced a total of 10,000 values of the standoff height, which were used to create Figure 3.21.

For comparison purposes, just the time to acquire data by the microchip's ADC, at a sampling rate of 6.25 kHz, with a scan width of 400 steps (200 μm) and a standoff height resolution of 2 steps (1 μm) will be looked at when analyzing this data. The time to acquire data after the standoff height of the global maximum levels out at 160 would be <5.12 seconds. To try to achieve both a short scan time and accuracy of the standoff height that produced the strongest signal intensity value, a location on the curve was looked for that corresponded to the calculated reference value with fewer samples averaged at each data point of the fine scan. Two such locations were found, one at 15 samples averaged (the blue arrows in Figure 3.21) and another at 25 samples averaged (the red arrows in Figure 3.21).

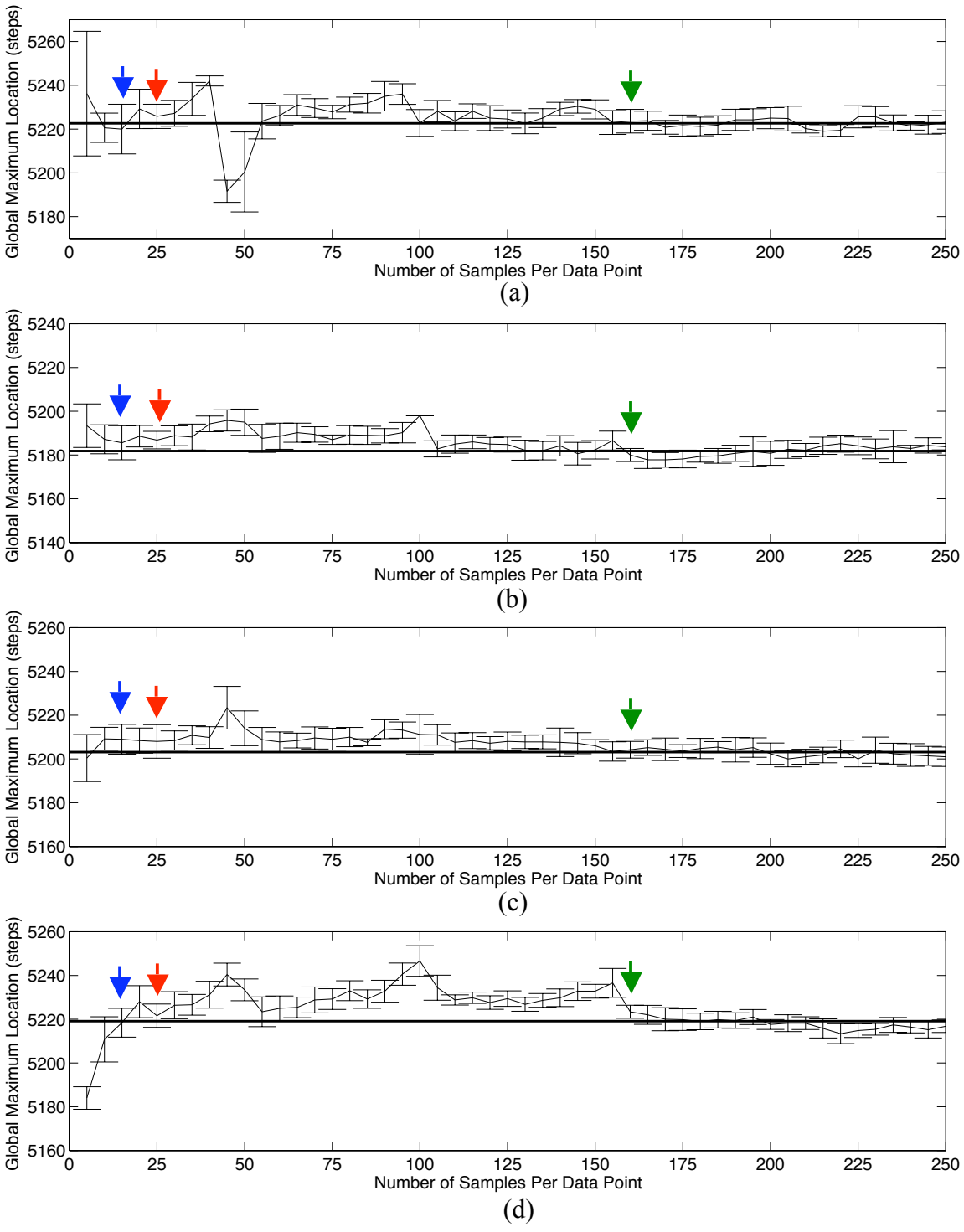

Figure 3.21: The effect the number of samples averaged has on the standoff height of the global maximum. Bold line shows long-term average, arrows indicate out points of interest.

Both locations were consistently close to the calculated reference value with significantly fewer samples needed to be averaged. With 15 and 25 samples averaged, the data acquisition time would be 0.48 and 0.80 seconds respectively. The average of the absolute difference from the 4 data points to their calculated reference value for both 15 and 25 samples averaged at each data point was 3.3 and 3.8 steps (1.7 and 1.9 μm) respectively. This error for both is very close to each other and with such a small sample size is not very meaningful. Because of this, the average of the standard deviations were calculated for 15 and 25 samples averaged at each data point to be 8.1 and 5.6 steps (4.1 and 2.8 μm) respectively. From the scan time, error, and standard deviation data, the number of samples to be averaged was chosen to be 25 to achieve a short scan time and accuracy with a stronger emphasis on accuracy shown in the lower standard deviation. In comparison to the data at 160 samples averaged at each data point with an average error of 2.2 steps (1.1 μm) and the average standard deviation of 3.8 steps (1.9 μm), the error increased by 1.6 steps (0.8 μm) and the standard deviation increased by 1.8 steps (0.9 μm) for a decrease in scan time of 4.32 seconds, a 640 % reduction in time with a very little decrease in accuracy.

The scan width was dependent on the surface finish of the chip type being focused on. For this study, the chip type that was being concentrated on was the flip chip. The size of the scan width will be larger for rougher surfaces and smaller for smooth surfaces. The scan width was determined experimentally by having the system adjust to find the best signal intensity strength on the surface of the chip and report the standoff height of the global maximum. The stage then moved the chip 0.457 mm (the solder ball pitch of the flip chip being tested on), and then the system readjusted and reported the standoff height of the new global maximum. The absolute difference between these two standoff heights was then calculated. This was repeated to find 188 results for each of the two flip chips being focused on giving a total of 376 results. The average difference from scan-to-scan of a flip chip was found to be ±97.3 steps (48.7 μm) with a standard deviation of 102.4 steps (51.2 μm). For a confidence interval of 95%, the scan width would have to be 596 steps (298 μm), and for a confidence interval of 99%, the scan width would have

to be 722 steps (361 μm). To achieve a 95% confidence interval, the scan width of the signal intensity adjustment algorithm was chosen to be 600 steps (300 μm).

With these parameters of a standoff height resolution of 2 steps (1 μm), 25 samples of the signal intensity strength averaged at each data point, and a scan width of 600 steps (300 μm), the average readjustment time was found to be 2.1 sec. This time will vary slightly on how far the focusing head has to move from the end of the fine scan to where the standoff height of the global maximum was found.

Automated Signal Intensity Adjustment System Interface

An important quality of the automated signal intensity adjustment system is its ease of use and adaptability. As seen in the previous section on the adjustment system algorithm, there are several parameters that control the accuracy and time of the scan. Some of these parameters are controlled by the vibrometer and its inherently noisy signal intensity strength output. Others, like the scan width, are dependent on the surface finish of the chip being inspected. With the automated signal intensity adjustment system being a stand-alone system, the interface to it is very important. The two forms of interface are a small tethered remote to allow an operator to directly command the system and a serial communication port for a software interface with a program like MatLab.

Remote for Operator's Commands

The remote is made from a plastic enclosure with three momentary switches panel mounted on the front and is shown in Figure 3.22. The remote uses the USB standard cable and plug to connect into the controller box, but it does not use the USB communication standards and should not be plugged into any other USB socket. The top button performs the standard readjustment of signal intensity strength with the parameters described in the previous section with a scan time of 2.1 sec. The middle button performs a readjustment with a wider scan width of 1000 steps (500 μm) with a scan time of 3.5 sec. This width corresponds to four times the standard deviation of the scan-to-scan difference in standoff height of the global maximum for a flip chip giving a 99.99% probability of finding the new standoff height of the global maximum. The bottom button performs the initial adjustment of the signal intensity strength with a scan time of

8.9 sec. All three buttons are programmable and could be programmed to any pre-desired set of scanning parameters that are needed with changing research needs.

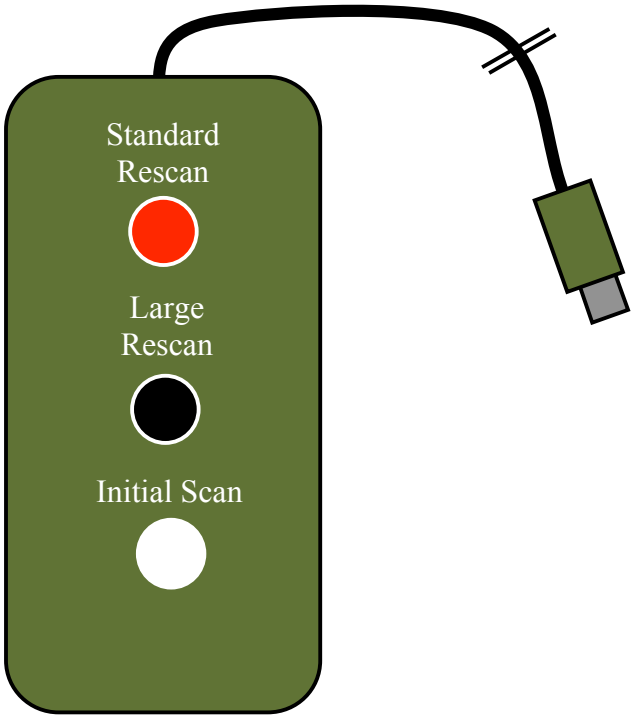

Figure 3.22: Tethered remote for operator's commands.

Software Interface With MatLab

To increase the flexibility of the automated signal intensity adjustment system, all of the parameters can be changed through a serial port from MatLab. Commands over serial can set the scan width, center point of the scan width, number of samples averaged during the initial scan, number of samples averaged during the fine scan, standoff height resolution of the initial scan, standoff height resolution of the fine scan, and the command to start either an initial adjustment or readjustment.

The final command that can be given is to take a reading of the signal intensity strength and return the value over serial. This could be used to determine if readjustment is needed after a move of the chip, reducing the time by eliminated unneeded adjustments. The acceptable signal intensity strength will depend on the type of chip

package. As seen in Figure 3.14, the achievable signal intensity could be higher for flip chips than it was for the BGA package.[17] For example, for a flip chip, a signal intensity value of 2.7 V and higher is a good signal.

These parameters can be tailored to the precise signal intensity strength adjustment needs for a variety of situations. For example, if this were used in an online inspection application, the geometry of the device being adjusted would be known. This means that the standoff height of the initial global maximum could be found once for the first unit, and then used for all consecutive units measured, removing the need to conduct an initial scan for each unit, saving time. Another example is if the system was focusing onto a polished silicon wafer, the scan width could be much narrower due to the smoothness of the surface, greatly reducing the rescan time.

Along with receiving commands over serial, the automated signal intensity adjustment system also sends data after each scan. This data gives the signal intensity strength that was found and its location in steps from the home position of the focusing head (standoff height).

CHAPTER 4

EXPERIMENTAL RESULTS USING AUTOMATED SIGNAL INTENSITY STRENGTH ADJUSTMENT SYSTEM

Results of Reliability Test

To validate the repeatability and functionality of the automated signal intensity strength adjustment system, a test was conducted with the adjustment system in conjunction with the rest of the nondestructive inspection prototype on a set of chips. Experiments were performed using a flip chip test vehicle PB18 without underfill. The die size is 6.35 mm × 6.35 mm and has a typical solder ball diameter of 190 µm with a pitch of 457 µm, with twelve solder balls located on each side of the chip. This test vehicle has 10 flip chips on each board numbered from chip 1 to chip 10, as shown in Figure 4.1 (a). Figure 4.1 (b) shows an illustration of the known defects in chips 1-3.

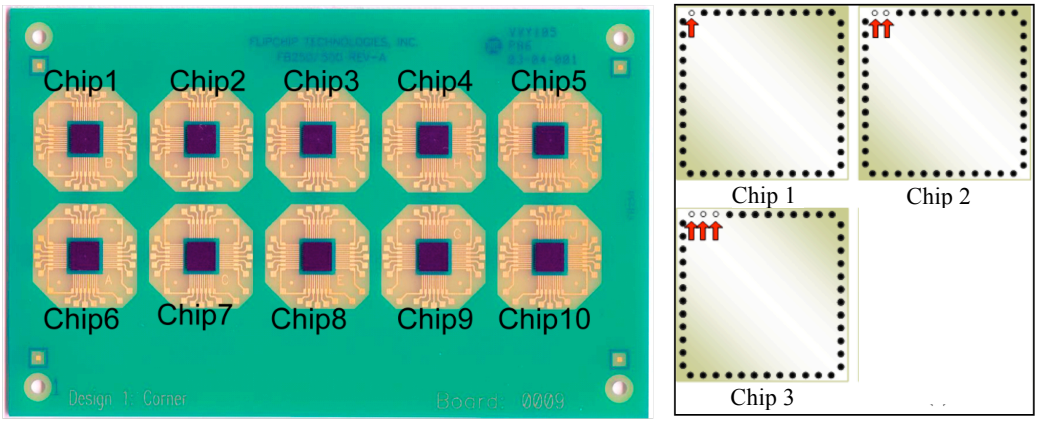

(a) (b)

Figure 4.1: PB18 test vehicle used for validation (a), illustration of known defects (b)

A set of flip chips were attached with one to four adjacent open solder balls starting from the top left corner of each flip chip, as shown in Figure 4.1 (b). The white circles indicate the locations of open solder balls. To create these open solder balls, individual solder pads were removed from the PCB. When the chips were soldered to the PCB, there was no metal to attach to for these solder balls, leaving them open. In Figure 4.1 (a), chips 4,

5, and 8 are good; while chips 1, 2, and 3 have one to three open solder balls beginning from the left top corner of the die. Chips 6, 7, 9 and 10 are omitted in this work.

The nondestructive measurement system test procedure for the chip was to use a vision camera to determine the precise location and orientation of the circuit board on the motion stage. The flip chip had 48 solder balls around the perimeter of the chip, 12 on each side. For the nondestructive test, the motion stage would position the chip so that the laser vibrometer would be focused on the top surface of the chip directly above the first solder ball. The YAG pulsed laser was incident the top surface of the chip directly adjacent to the vibrometer laser spot location. The pulsed laser induced vibration in the chip and the vibrometer recorded the vibration. The motion stage would then move the chip 457 μm (the pitch of the solder balls) to the next solder ball and repeat the measurement process. This process would be repeated counterclockwise around the chip until all 48 solder balls had been measured.

For the validation testing, this nondestructive test procedure was used, but instead of capturing the vibration data at each solder ball, the signal intensity strength and standoff height data was captured. For each of the 48 solder ball locations of chip 1 and chip 2, the automated signal intensity strength adjustment system performed an initial adjustment. An initial adjustment was conducted instead of a readjustment to allow both portions of the signal intensity strength adjustment algorithm to be tested and to give more consistency of the scan type for comparison purposes.

The test procedure was conducted as follows: the circuit board was optically aligned, signal intensity strength adjustment was done on chip 1, signal intensity strength adjustment was done on chip 2, signal intensity strength adjustment was done on chip 1 and then chip 2 again with no change in alignment. The following day this procedure was repeated including the removal and replacement of the circuit board and its optical realignment. This gave a total of 4 sets of signal intensity strength adjustment data for each of the 2 chips. Figure 4.2 gives the results of the repeatability test.

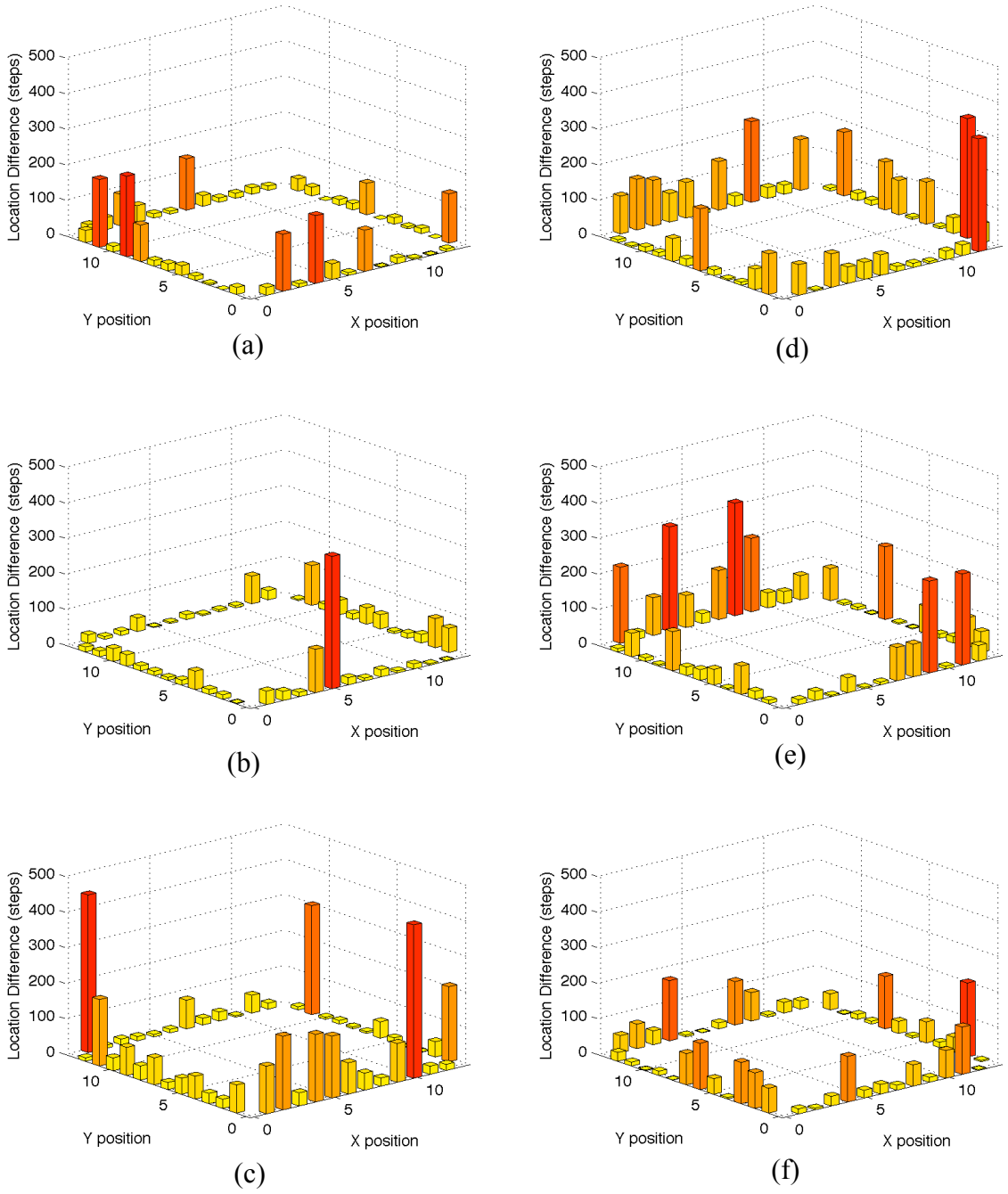

Figure 4.2: Differences between standoff height for 2 flip chips for comparison purposes. (a)-(c) show comparisons of chip 1 and (d)-(f) show comparisons of chip 2.

The graphs in Figure 4.2 show the absolute difference between measurement procedures of a specific chip. Graphs (a)-(c) are of chip 1 and graphs (d)-(f) are of chip 2. The X and Y axes give the coordinates of the inspection locations on the chip, which correspond

to the solder ball locations. Graphs (a) and (d) show the absolute difference in the standoff height of the global maximum of the signal intensity strength profile of each of the 48 inspection locations between the two testing procedures performed on the first day. Graphs (b) and (e) show the absolute difference in the standoff height of the global maximum of each of the 48 inspection locations between the two testing procedures performed on the second day. Graphs (c) and (f) show the difference between the first and second day test results. The first day's average standoff height of the global maximum of each of the 48 inspection locations was found from the two tests run the first day, and a second set of averages was found from the two tests run the second day. The absolute difference between these two averages is what is shown in graphs (c) and (f). In graphs (a), (b), (d), and (e) there was a large difference. In graph (d) there were 31% of the measurements that had a difference larger than 100 steps. Comparing graphs (a) to (b) and (d) to (e) the differences were not consistent from the first day to the second. Graph (c) and (f) show that the large percentage of differences also appeared in the differences from the first day to the second. Graph (c) shows that for chip 1 the differences from the first day to the second were much larger and more numerous than the differences on either of the individual days.

Interpreting the Results

To understand where the inconsistencies in the global maximums were coming from, a series of tests was conducted to isolate and understand the results in Figure 4.1. These tests varied the different individual elements of the measurement system that could introduce error to determine which had the largest effect on the consistency of the global maximum. Chip 1 was used in the detailed investigation below.

The first component of the signal intensity strength adjustment system that was investigated was the repeatability of finding the standoff height of the global maximum of the signal intensity strength profile without any movement of the chip by the positioning stage and is shown in Figure 4.3.

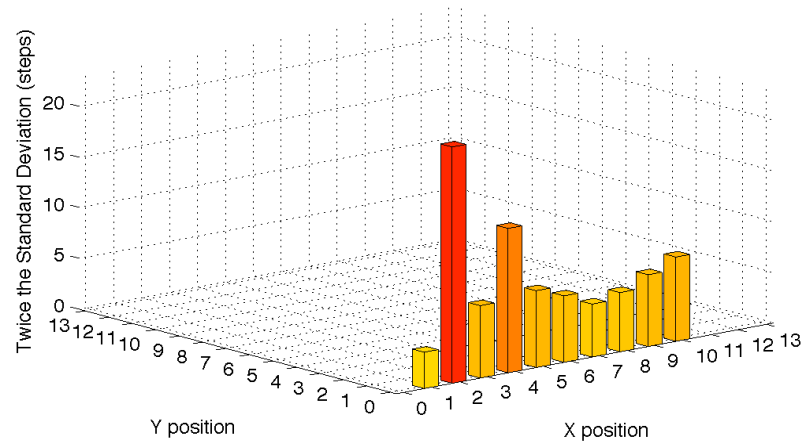

(a)

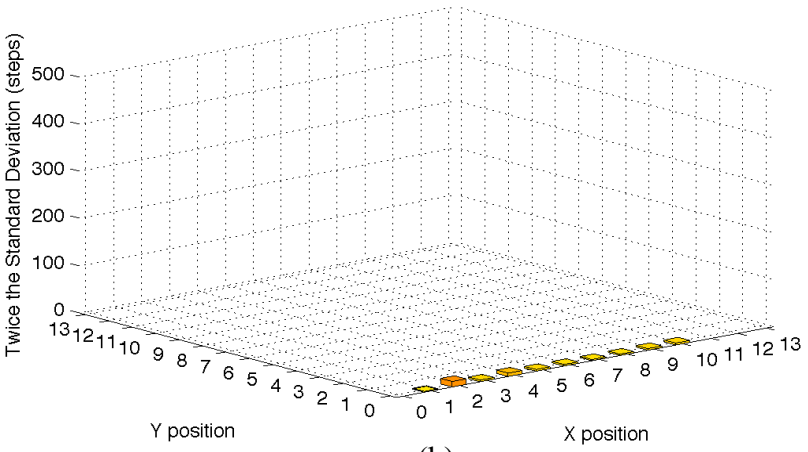

(b)

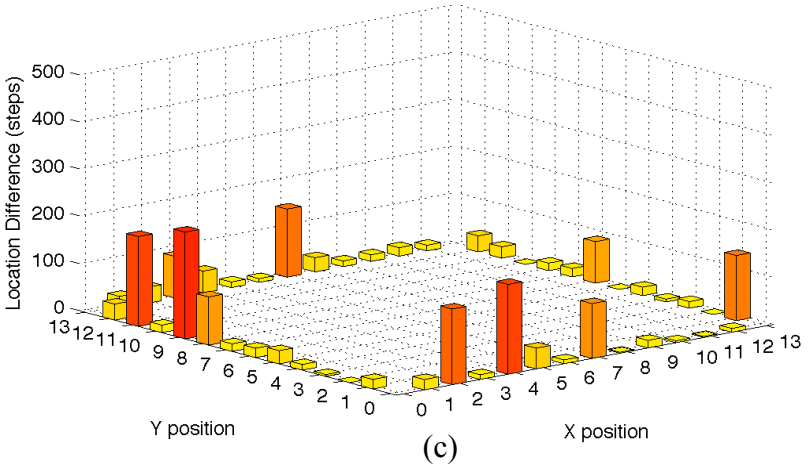

(c)

Figure 4.3: Repeatability of finding the standoff height without movement of chip. (a) and (b) show variation of the global maximum. (c) shows difference graph from Figure 4.1 (a) for comparison.

The first ten focusing locations on chip 1 were investigated. The stage moved the chip into the proper location for inspection; the adjustment system then conducted five consecutive initial adjustments of the chip at that location. This removed any variation in the exact inspection location leaving the only variation in the vibrometer adjustment system. Graph (a) of Figure 4.3 shows twice the standard deviations (95% confidence interval) of the standoff height found at each of the first ten inspection locations on chip 1. Graph (b) shows the same data found in (a) but at the same scale as the difference graph (c), which is the same graph as Figure 4.2 (a) shown here for comparison purposes. As seen in graph (c), the two focusing locations with the largest difference (when only looking at the first 10 locations) are at location 2 and 4. These two locations also correspond to the two locations in (a) with the largest standard deviation. When comparing (b) to (c), it is very clear that the vast majority of the variation is coming from a source other than the vibrometer adjustment system itself. The variation in the vibrometer adjustment system seen in (a) can be accounted for in the inherently noisy signal intensity strength input as seen in Figure 3.10. Along with this, the differences in the specularity of the surface being focused on at each location will greatly affect the signal intensity strength adjustment repeatability that can be achieved.

The second component that could have produced differences in the test results was the motion stage, which had a resolution of 0.2 μm. The repeatability of the stage directly controls the repeatability of the location at which the vibrometer is inspecting at on the chip's surface. The bidirectional repeatability of the stage was experimentally found to be ±6 μm[10]. To understand how the variation in exact inspection location on the chips surface can affect the standoff height found at the global maximum of the signal intensity strength profile, a test was conducted to investigate what variations in the global maximum are present within the ±6 μm window of where the motion stage could have placed the chip. Figure 4.4 shows a set of global maximums within a ±6 μm window of two of the inspection locations on chip 1, location 9 and 11. To make the differences in height of Figure 4.4 more apparent, all the values are shown relative to the lowest value.

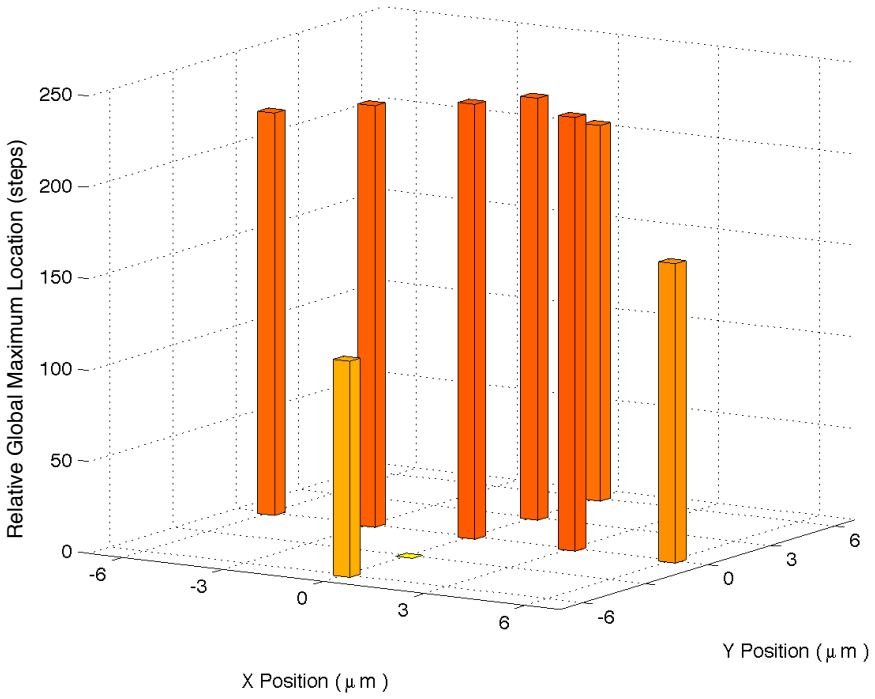

(a)

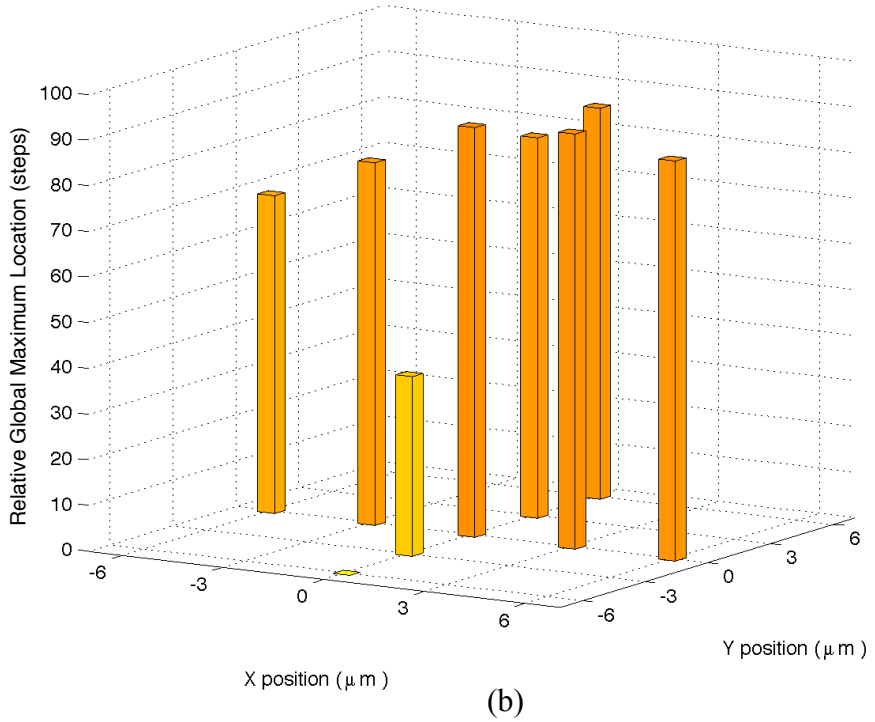

(b)

Figure 4.4: Relative standoff heights within a ±6 μm window on chip 1. (a) at location 9 and (b) at location 11.

For this test, the positioning stage placed the chip at location 9 for (a) and location 11 for (b). The vibrometer adjustment system conducted 10 consecutive adjustments at that location. The stage then moved the chip 3 μm and then 6 μm in both directions from the initial data point on the X and Y axes creating a cross-shaped pattern of data points around the initial location. The 3 μm intervals of the data came from the vibrometer laser's minimum spot size of 3 μm.[16] These samples show a set of alternate locations the vibrometer laser could have been inspecting, given the repeatability of the stage. For Figure 4.4, each sample data point shows the average standoff heights of the 10 adjustments at each location. These values were then shown relative to the lowest value. Figure 4.4 clearly shows a very large variation in the standoff height within the ±6 μm window for a flip chip. For (a) the largest difference was nearly 240 steps (120 μm) and (b) the largest difference was over 90 steps (45 μm). This was shown to be the primary cause of the variation seen in Figure 4.2.

Given that the standoff height varied so greatly over the statistically possible locations the measurement could be taken at, the signal intensity values where also investigated to see if this variation also applied to their values. Figure 4.5 shows the signal intensity values from the same test conducted for Figure 4.4. The signal intensity values were seen to vary considerably over the statistically possible locations. For graph (a) the signal varied from a low of 1.9 V to a high of 3.3 V. These signal levels correspond to a poor signal and a very strong signal. Variations were also seen in (b) with a low of 2.5 V and high of 3.6 V, corresponding to a good signal and a very strong signal respectively. Figure 4.5 shows the importance of controlling both the exact location where the vibrometer is inspecting and the standoff height that achieves the strongest signal intensity. If a strong enough signal intensity cannot be found with the first readjustment of the vibrometer, a search pattern around the desired location can be used to find a location that gives a stronger signal intensity.

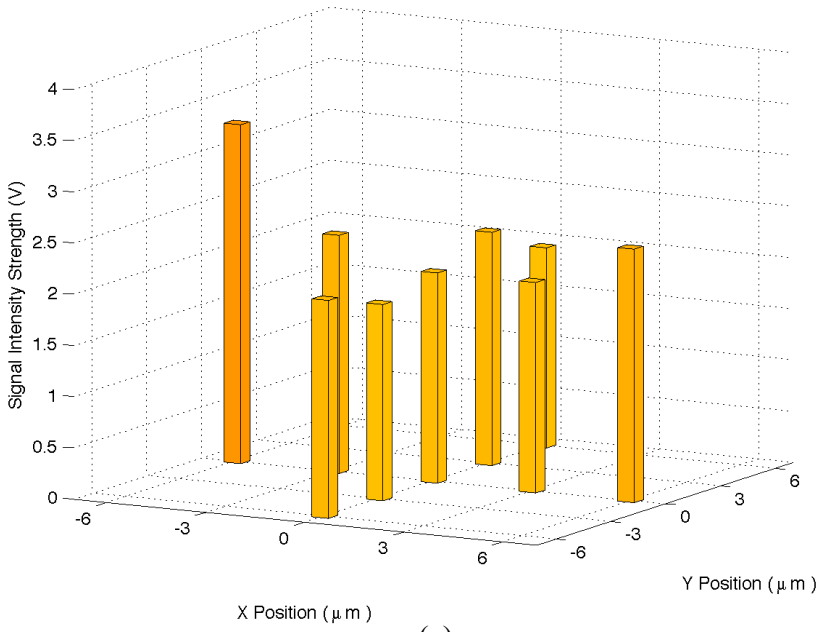

(a)

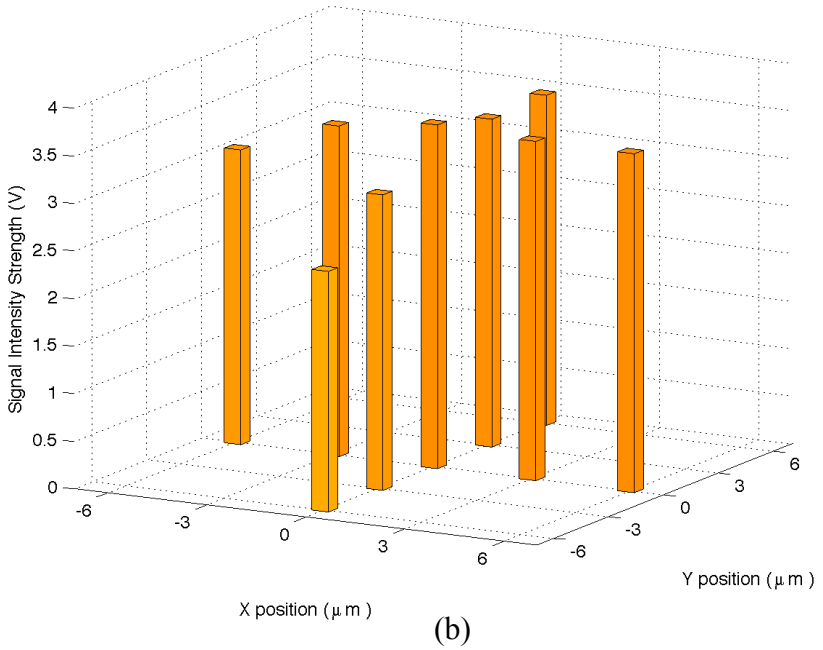

(b)

Figure 4.5: Vibrometer signal intensity levels within a ±6 µm window on chip 1. (a) at location 9 and (b) at location 11.

For the flip chip that was being investigated, the solder bump diameter was 190 μm. With the search pattern of ±6 μm being much smaller than the solder bump, the use of these alternate locations would not significantly alter the results of the signal processing method used in the nondestructive inspection analysis[10].

To further validate that the variations in standoff height were coming from the surface finish of the flip chip, the test that was conducted in Figure 4.2 was repeated on a polished silicon wafer with a surface roughness of 1 nm, and is shown in Figure 4.6. The scale for the location difference is held constant for comparison purposes.

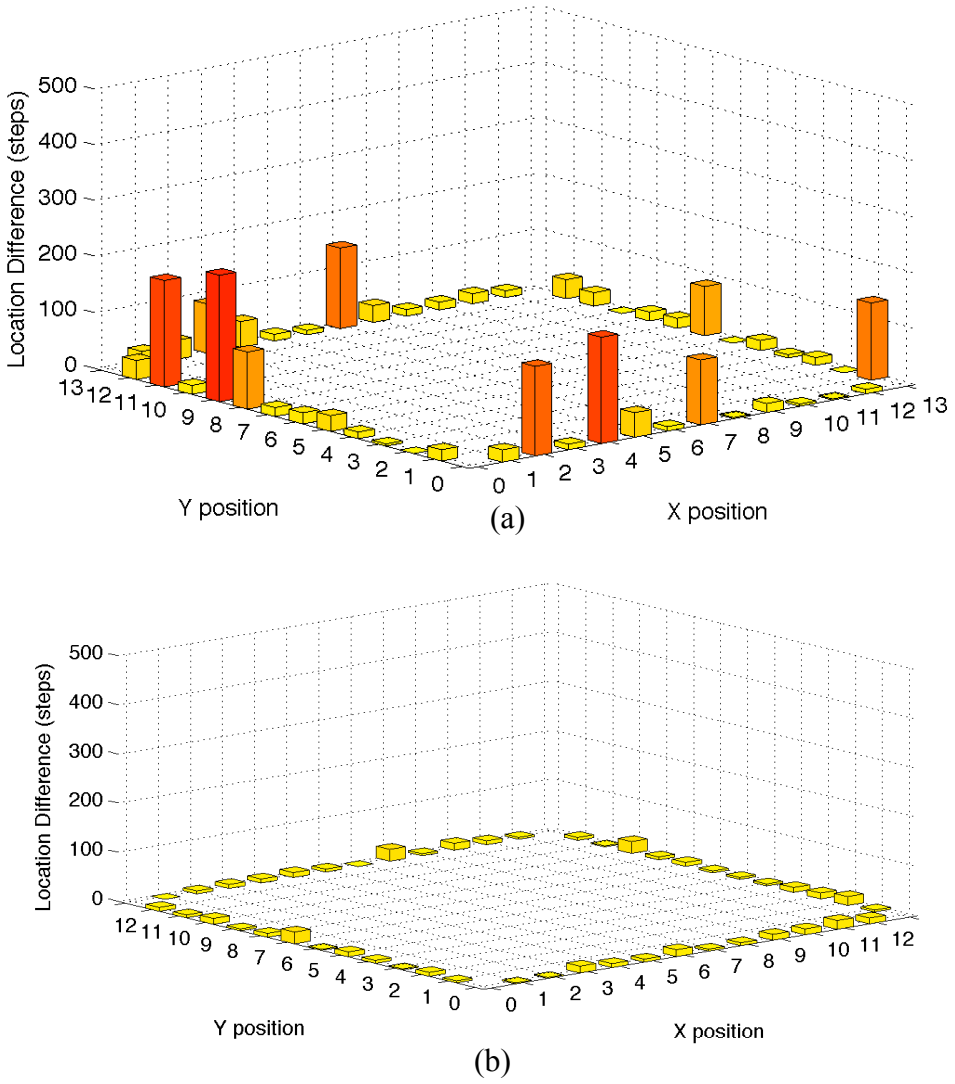

Figure 4.6: Differences between standoff height, flip chip (a), silicon wafer (b).

Plot (a) of Figure 4.6 is the same plot as Figure 4.2 (a) shown here for comparison. When the repeatability test was conducted on a smooth silicon wafer, the large variations that were present with the flip chip were not found, as seen in Figure 4.6 (b).

In addition, the test that produced the results seen in Figures 4.4 and 4.5 were repeated on the silicon wafer, seen in Figure 4.7. The scales were held constant with those used in Figures 4.4 and 4.5 for comparison purposes. For plot (a), all the values are shown relative to the lowest value to show the difference in height more clearly.

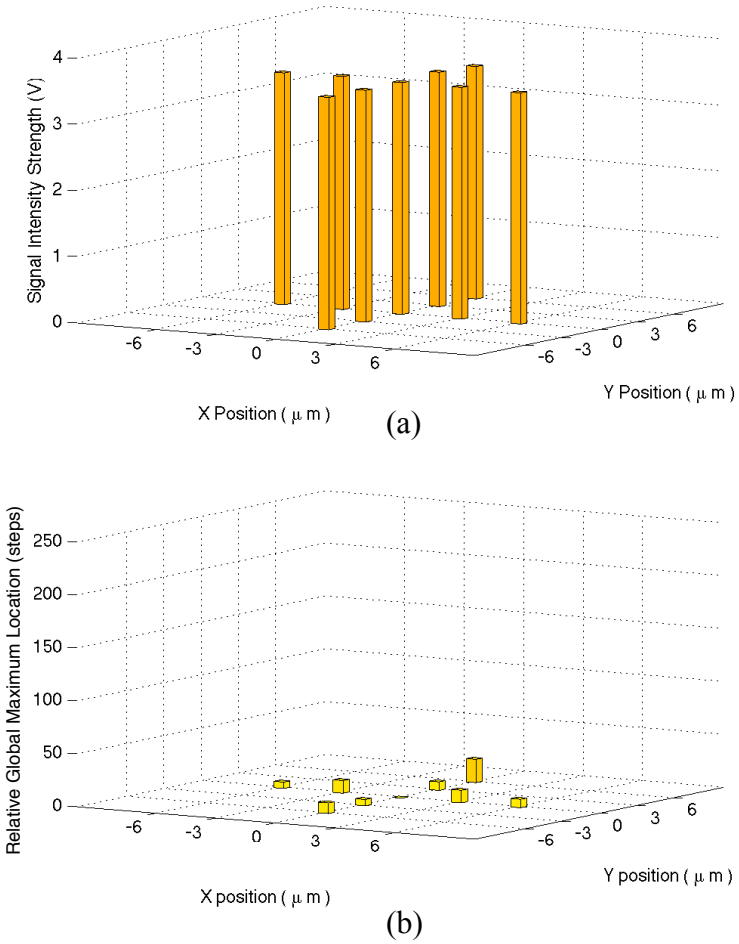

Figure 4.7: (a) Signal intensity strength and (b) relative standoff heights within a ±6 μm window on silicon wafer.

As seen in Figure 4.7 (a), the signal intensity strength within a ±6 μm window is very consistent with a minimum of 3.49 V and a maximum of 3.54 V. The same small variations are also found in Figure 4.7 (b) where the max difference in standoff height

was found to be 22 steps (11 μm). When compared to Figure 4.4 with a flip chip, which has a max difference in standoff height of over 200 steps (100 μm), it is clear that the surface roughness when combined with the repeatability of the X-Y positioning of the IC was the reason for the variations in Figure 4.2. This test conducted on a silicon wafer also further strengthens the reliability of the data seen in Figures 4.4 and 4.5, which indicated the need to search for an alternate inspection location when the surface is rough.

CHAPTER 5

AUTOMATED SIGNAL INTENSITY STRENGTH ADJUSTMENT SYSTEM VALIDATION

Validation of Quality of Results

To validate that the automated signal intensity strength adjustment system would improve or maintain the speed and repeatability of the nondestructive inspection prototype, the vibrometer adjustment system was used in the capturing of data, and the defect detection results were compared for consistency. The results were also compared to the previous results when adjusting the vibrometer manually.

To demonstrate the capability of the signal intensity strength adjustment system to be fully automated and able to be integrated into the nondestructive inspection prototype, a MatLab script was written to control both the positioning stage and the vibrometer adjustment system together. The script allowed a fully automated positioning system that would move the chip to the proper location for data to be taken, the vibrometer would be adjusted on that location, and then instruct the operator to acquire data. A single click would move the chip to the next location and adjust the signal strength. From the results of the repeatability test of just the signal intensity strength adjustment system above, it was learned that the exact location being inspected was important to control to consistently obtain a strong vibrometer signal intensity. To achieve this, the script would move the chip to the initially desired location. The signal intensity strength was measured by the vibrometer adjustment system and if the signal strength was above a preset threshold, the system would not adjust and immediately instruct the operator to capture data. If the signal strength was below the threshold, the system would readjust to find the standoff height that correlated with a stronger signal intensity. If the signal strength was above the threshold, the script would instruct the operator to capture data. If the signal strength was still below the threshold, the script would start moving the chip to attempt to locate an alternate inspection location that would produce a stronger signal, similar to that seen in Figure 4.5. The search pattern was in a spiral pattern starting at the original location and spiraling out in a 1 μm grid. The grid was ± 3 μm corresponding to half the repeatability of the position stage, producing 48 alternate test locations. As the script

moves from location to location, the signal strength would be measured; if above the threshold, the search would stop and the script would instruct the operator to capture data. If the signal strength with still below the threshold, the script would move the chip on to the next location in the spiral grid. Every 4th alternate location, the system would readjust to attempt to maintain the proper standoff height while minimizing searching time. If on completion of the pattern a value above the threshold was not found, the stage would move the chip back to the location where the strongest signal was found, readjust, and instruct the operator to capture data.

The validation was performed using a flip chip test vehicle PB18 without underfill shown in Figure 4.1. There were six chips that were used in the validation, chips 4, 5, and 8 as the good chips and chips 1, 2, and 3 have one to three open solder balls beginning from the left top corner of the die as the defective samples. Chips 6, 7, 9 and 10 are omitted in this work. The repeatability of the inspection prototype can be seen in Figure 4.7, Figure 4.8, and Figure 4.9, which show the correlation coefficients, the measure of consistency, between two tests performed on consecutive days.

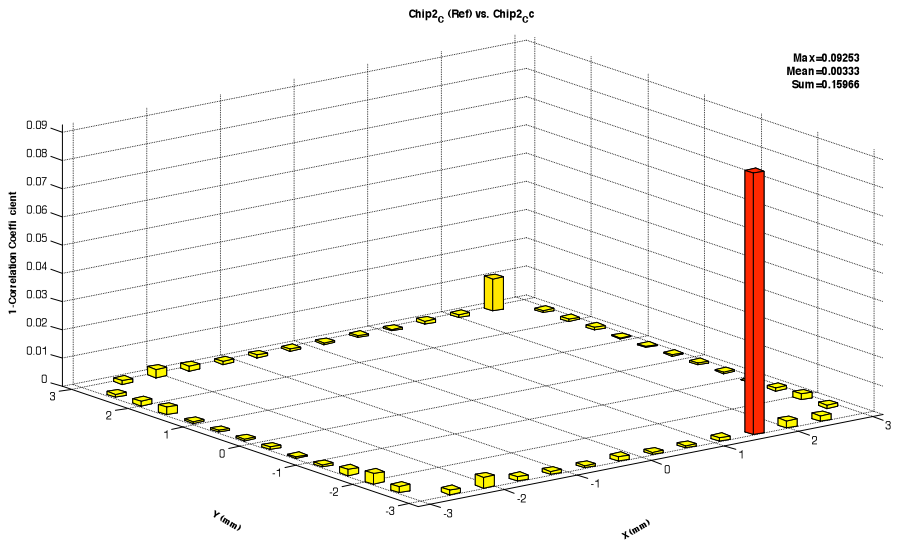

Figure 5.1: Repeatbility of data captured on chip 2 shown as a correlation coefficient at each test location.

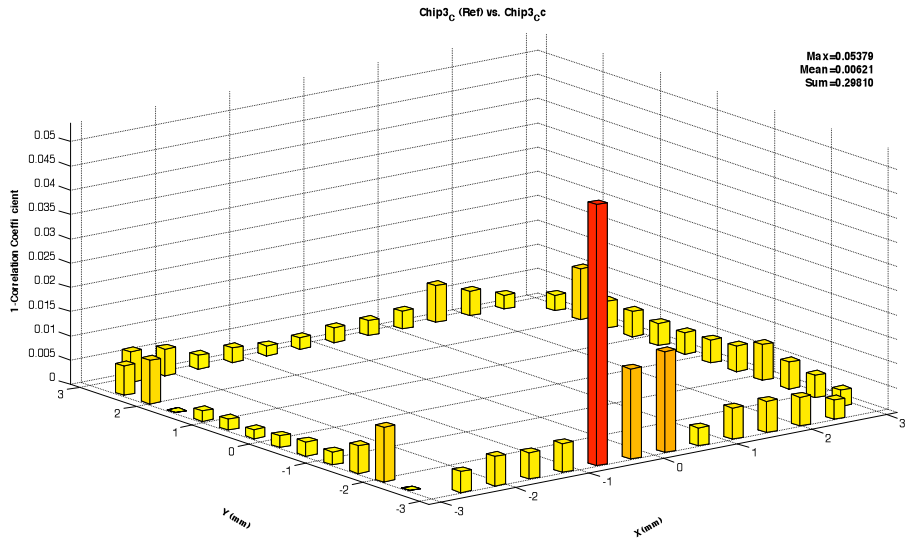

Figure 5.2: Repeatbility of data captured on chip 3 shown as a correlation coefficient at each test location.

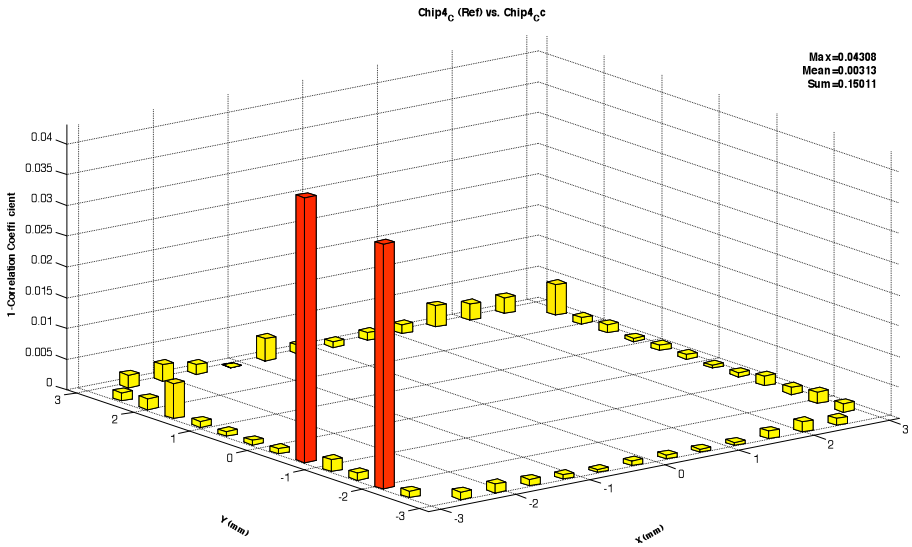

Figure 5.3: Repeatbility of data captured on chip 4 shown as a correlation coefficient at each test location.

Because of the immaturity of the software, several test locations have a relatively large dissimilarity. Despite this fluctuation, all the means and maximums are in the same scale. To reduce the effect of relatively big fluctuations, the mean of the correlation coefficient was used as the device signature of the device quality. The three means of repeatability test range from 0.0033 to 0.0062. Figure 5.4 shows the results of the defect

inspection system for three known good (chips 4, 5, and 8) and three known bad (chips 1, 2, and 3) flip chips. To compensate for manufacture variation and quality degradation of the three good devices, a hybrid signal was generated by the signal from the three good devices to be used as a comparison reference.

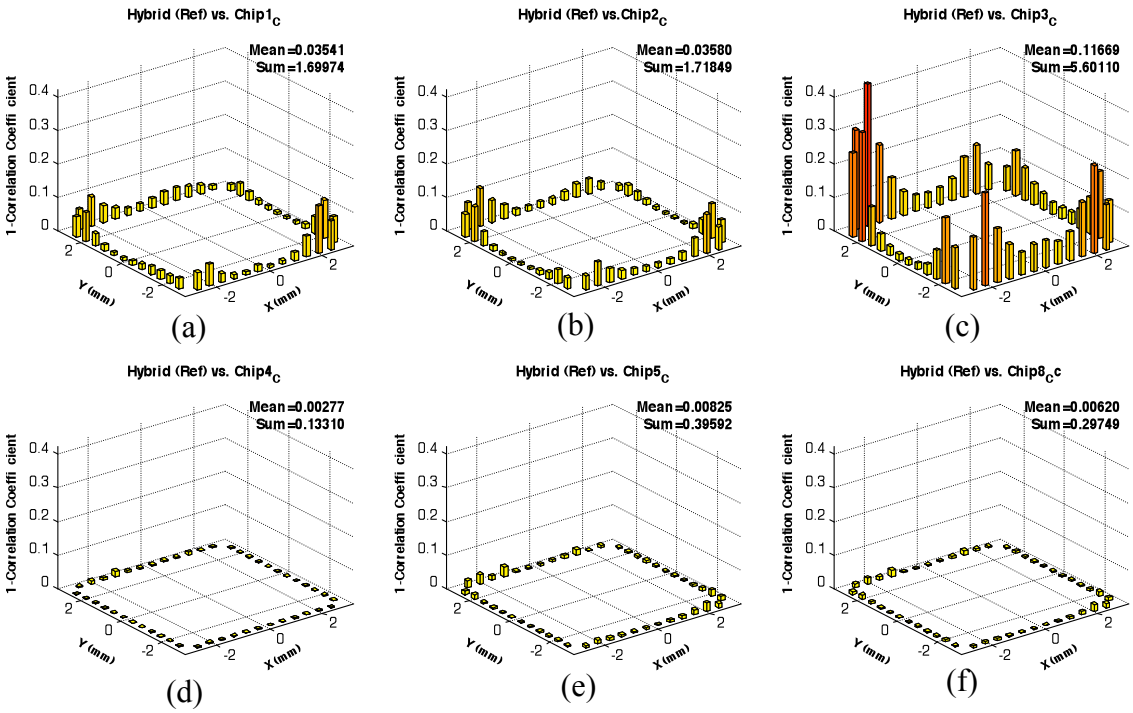

Figure 5.4: Results of inspection prototype validating ability to distinguish defective chips when using automated vibrometer adjustment. (a)-(c) are defective chips. (d)-(f) are good chips.

It is very easy to distinguish the defective devices from the good ones with the large difference in means as shown in Figure 5.4. The means for good chips ranged from 0.0027 to 0.0083, while the bad chips ranged from 0.0354 to 0.1167 with the mean rising with the number of defects. This large difference in range from good to bad chips is an order of magnitude out of the range of repeatability as seen in Figures 5.1 through Figures 5.3 as 0.0033 to 0.0062, which indicates this difference was caused by the defect instead of experimental error. Figure 5.5 shows the ability of the inspection prototype to detect defects when the vibrometer was adjusted manually by a skilled operator.

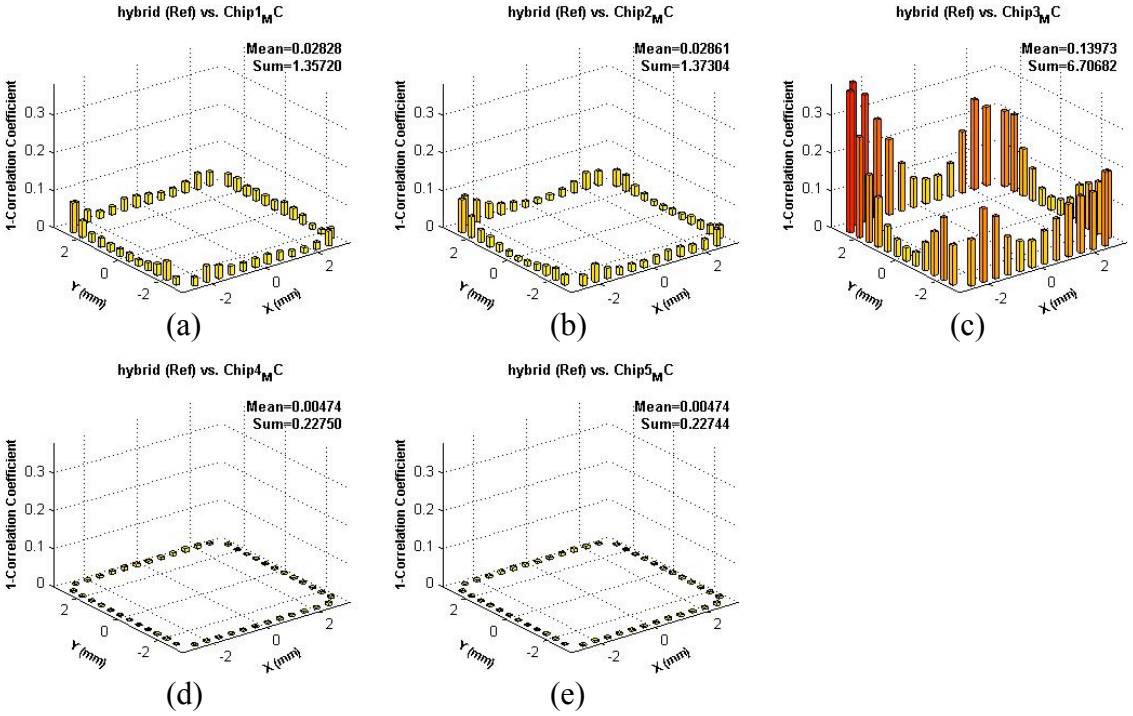

Figure 5.5: Results of inspection system distinguishing defective chips from good chips when manually adjusting vibrometer. (a)-(c) are defective chips. (d)-(e) are good chips.

When comparing Figure 5.4 to Figure 5.5, it is seen that the results are similar. The mean for good chips was in the area of 0.0047, while the bad chips ranged from 0.0283 to 0.1397 with the mean rising with the number of defects. Both the good and bad chips fall into the same correlation coefficient range with consistent patterns for both the manual and automated adjustment of the vibrometer. This shows that the fully automated signal intensity adjustment system can produce results similar to those performed by a skilled operator.

Reduction in Data Acquisition Time

For manual adjustment of the vibrometer, the time depends on how long it takes the operator to find a strong signal, which is described in more detail in Chapter 2 under system limitations, and the number of problematic inspection locations. For the automated vibrometer adjustment system, variation comes again from the number of difficult inspection locations. For both methods, the capturing of the data is currently done manually, which introduces more variation based on the speed and skill of the

operator. With manual adjustment of the vibrometer, data acquisition took approximately 72 sec per test location. The variation in the automated vibrometer adjustment system was easier to quantify by having the MatLab script record the adjustment time automatically. The adjustment time data was calculated from 144 trials. It was found that 32% of the time, the signal strength was already above the threshold not requiring any adjustment of the vibrometer and only requiring 0.5 sec before capturing data. In 21% of the time, readjusting the vibrometer on the original location raised the signal strength above the threshold, requiring 2.7 sec before capturing data. For 47% of the time, an alternate inspection location had to be searched for. This required 3.7 to 71.0 sec to find a signal strength above the threshold, depending on how far into the search pattern it was located. The average time to acquire a strong signal strength was 7.4 sec. Figure 5.6 shows a histogram with 2 second bins of the required adjustment times to find a strong signal strength and the percentage of their occurrence out of the 144 trials.

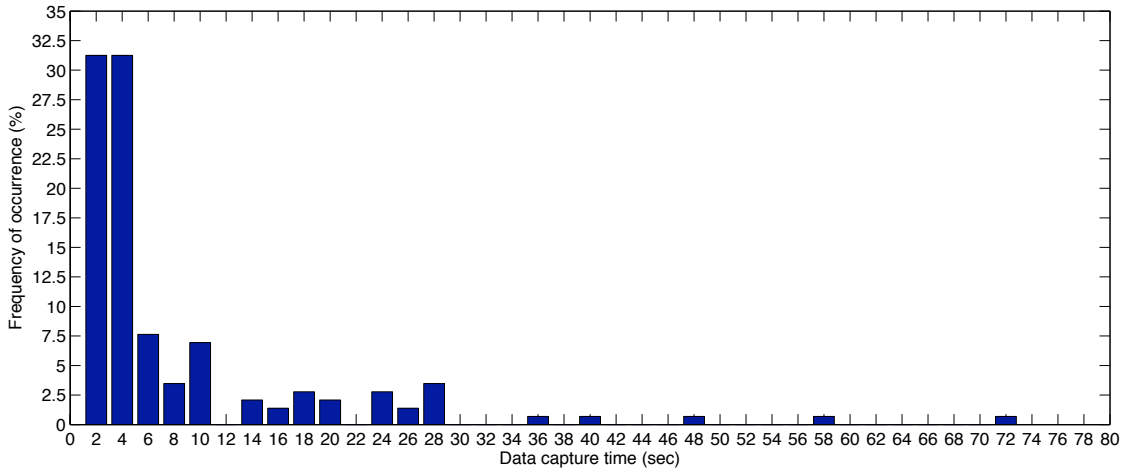

Figure 5.6: Histogram of required adjustment times and the percentage of their occurrence.

As seen in Figure 5.6, the majority of the adjustment times are short. Over 67% of the time, the adjustment time was less than 5 sec and approximately 90% of the time it was less than 20 sec. The minimum adjustment time was 0.5 sec and the maximum was 71.0 sec. The maximum time has a large opportunity for improvement by further modifying the search pattern to optimize for specific chip package surfaces. With the time to capture data manually being approximately 8 sec, the time to capture data per test

location was found to be a minimum of 8.5 sec and maximum of 79.0 sec with an average data capturing time of 15.4 sec. When compared to the time required to capture data by hand by a skilled operator, the improvement in speed to the inspection system was almost 4 times. This time can still be further reduced by improving search patterns, using a faster and more precise positioning stage, and by using a laser with a faster pulse rate to reduce the time needed to capture data. With the full automation of all the nondestructive inspection prototype components, the acquisition time should be able to be further reduced by removing more human variation.

CHAPTER 6

CONCLUSION

Expected Impact of Research

The long-term goal of this research is to assist in the development of a fast, accurate, and low-cost non-destructive inspection prototype system. The ability to perform the inspections in an automated manner is very important in order to demonstrate the ability of the system to be used for online inspection. By removing the need to manually adjust the laser vibrometer, the inspection prototype will be able to be fully automated. To arrive at this goal, the development of an automated signal intensity adjustment system was developed. It was shown that the quality of results with the automated vibrometer adjustment system was similar to that when the vibrometer was being manually adjusted by a skilled operator. The shorter adjustment time that was achieved by the automated vibrometer adjustment system increased the speed of the overall inspection prototype by approximately four times with a minimum data acquisition time of 8.5 sec and an average time of 15.4 sec, allowing the data to be captured faster from the IC chip, which will increase the throughput and quality while reducing the cost of the products being inspected. This would both be beneficial to the producer as well as to the end consumer.

The removal of human error in manual adjustment of the vibrometer also makes the inspection prototype a more effective research tool by making the system more repeatable and easier to use. The effect of the operator's skill for manual adjustment of the vibrometer was removed, making the data more reliable when compared to results of tests made by different operators.

The flexibility of the signal intensity strength adjustment system to be able to be customized through a software interface like MatLab, allows the signal intensity strength adjustment system to be adapted to new IC package types and be easily modified for changing research needs.

Advantages and Limitation

The primary advantage to the automated vibrometer adjustment system described in this work over vibrometers with integrated autofocusing, like the Polytec OFV-505, for example, is the full control over the signal intensity adjustment parameters. With the Polytec OFV-505, the only control the user has is the command to autofocus and the ability to save focusing configurations and recall them. When the autofocus command is given to the Polytec unit, the system takes approximately 10 seconds to autofocus. With the retrofitted design described in this work, the adjustment parameters can be optimized for the characteristics of the surface being inspected. This is far superior to the generic focusing algorithms that use no knowledge of the surface. This is evident by the fact that the signal intensity adjustment system was able to find a strong signal intensity in 2.1 seconds, nearly five times faster than Polytec's commercial system.

Another important advantage to the vibrometer adjustment system described here is the ability to have all the adjustment parameters able to be changed and customized. The openness of its controls over serial communication allows it to be tightly integrated into automated inspection systems that can take full advantage of its flexibility for optimization purposes.

The primary limitation to further reducing the adjustment time is the inherently noisy signal intensity output of the vibrometer. With the use of a different vibrometer with a less noisy output of signal intensity, fewer samples could be taken at each data point when performing the fine scan seen in Figure 3.19. This would reduce the adjustment time greatly.

CHAPTER 7

RECOMMENDATION FOR FUTURE WORK

These are a few recommendations for further work that would improve the automated signal intensity adjustment system and its use.

Improved Search Patterns

As seen in Figure 4.5, there was found to be a large variation in the signal intensity over a very small area around the desired inspection location. This shows that to find a strong reading of the IC chip's vibration, the precise position of the vibrometer's laser on the IC is needed. The interface of the vibrometer adjustment system was developed for MatLab and a script was written that demonstrated the ability for the vibrometer adjustment system to be integrated into a fully automated inspection system. Further worked could be performed developing faster and more optimized algorithms for searching for alternate inspection locations with the full automation of the inspection prototype in place.

Characterization of Chip Package Surface Finish

An area of further research that would be beneficial to the vibrometer adjustment system would be further characterization of the surface of different chip packages. With control over the vibrometer adjustment system in MatLab, algorithms could be developed that incorporate the stage positioning and vibrometer adjustment system to determine the adjustment parameters in a fully automated way. This algorithm could perform the tests described in Chapter 3 for the development of the focusing parameters in an automated manner, returning the recommended parameters and showing the plots from which the recommendation was made. This would allow the system to adapt itself to changing surface characteristics of the IC chip and maintain a balance between refocusing time and accuracy.

REFERENCES

1) Rao R. Tummala, Eugene J. Rymaszewski, Alan G. Klopfenstein, Microelectronics Packaging Handbook: Semiconductor Packaging, Part II, 2nd edition (Boston: Kluwer Academic Publishers, 1997), II-12.

2) Charles A. Harper, Electronic Packaging and Interconnection Handbook, 3rd edition (New York: McGraw-Hill, 2000).

3) c <http://www.chipscalereview.com/archives/ES/issues/0801/tutorial_01.html> (2 June 2009).

4) Hem Takiar, "The Experts Look at the Issues: Forecast 2001: A look Ahead," Chip Scale Review, January-February 2001, <http://www.chipscalereview.com/archives/ES/issues/0101/f2_01.html > (2 June 2009).

5) Charles A. Harper, Electronic Packaging and Interconnection Handbook, 3rd edition (New York: McGraw-Hill, 2000), 8.72.

6) Stuart Wright, "X-Ray Inspection of IC Packages and PWBs," Chip Scale Review, August-September 2001.

7) Tom Adams, "Online Inspection for Hidden Internal Defects," Sensors, April 2000.

8) Sheng Liu, Dathan Erdahl and I. Charles Ume, "Vibration Analysis Based Modeling and Defects Recognition for Flip Chip Solder Joint Inspection", in Proceedings of the ASME International Mechanical Engineering Congress & Exposition (IMECE), Orlando, FL (5-10 November 2000).

9) Sheng Liu, Dathan Erdahl and I. Charles Ume, "A Novel Method and Device for Solder Joint Quality Inspection by Using Laser Ultrasound", in Proceedings of the 50th Electronic Components & Technology Conference, Las Vegas, NV (21-24 May 2000), 408- 415.

10) Turner A. Howard, "Design of an Advanced System for Inspection of Microelectronics Devices and Their Solder Connections Using Laser-Induced Vibration Techniques", (M.S. thesis, Georgia Institute of Technology, 2002).

11) C. B. Scruby and L.E. Drain, Laser Ultrasonics: Techniques and Applications (Bristol: Adam Hilger, 1990), 76.

12) "Specifications," in Vibrometer Operator's Manual for Polytec Vibrometer Series, Polytec GmbH, VIB-MAN-OFV2700-9411-e02, 7-4.

13) "Detailed Functional Description of the Interferometers," in Vibrometer Operator's Manual for Polytec Vibrometer Series, Polytec GmbH, VIB-MAN-OFV2700-9411-e02, chapter 5, 9-10.

14) "Detailed Functional Description of the Interferometers," in Vibrometer Operator's Manual for Polytec Vibrometer Series, Polytec GmbH, VIB-MAN-OFV2700-9411-e02, chapter 5, 1-7.

15) Joshua Vaughan, Aika Yano, William Singhose, "Comparison of Robust Input Shapers", *Journal of Sound and Vibration*, 2008; 315 p. 797-798.

16) Alexander D. Ryer, Light Measurement Handbook (Newburyport, MA: International Light, Inc., 1997), 13.